Computational Approaches to a Novel Orbital Problem

Andre Yu Tiamco

May 16, 2023

Contents

1 Introduction **1**

2 Experimental Procedure **2**
2.1 Generating Data 2
2.2 Describing the Bowl 4

3 Analytic Approach **6**
3.1 Orbital Mechanics 6
3.2 Our Problem 7
3.3 Problems with the Approach 7

4 Numerical Approach **8**
4.1 Simple Solution 8
4.2 Accounting for Decay 10
4.3 Using Paraboloid Fit 11

5 Machine Learning Approach **15**
5.1 Background on Neural Networks 15
5.2 Physics-Informed Neural Networks 16
5.3 The PINN Approach 16

6 Conclusion **18**

7 Appendix A: Raw Data **20**

8 Appendix B: Paraboloidal Numerical Path Data **22**

9 Appendix C: Neural Network Data **26**

1 Introduction

In studying the motion of a given mechanical system, one is often tasked with the derivation of certain rules or equations which this motion obeys. Through the implementation of such basics of physical principles as Newton's laws of motion (or through more complex forms of the same principles via Lagrangian mechanics or otherwise), it is, in the vast majority of situations, both possible and relatively easy to arrive at a set of ordinary or partial differential equations governing the behavior of the system. Then given the appropriate initial/boundary conditions, these equations uniquely determine the evolution of a system in time.

Despite the relative ease at which these governing equations can be derived, in practice, describing the motion in a way that is practical can be quite difficult. This is due to the inconsistency (and frequent impossibility) of finding analytic, closed-form solutions to differential equations (DEs). As a result, computational

approaches often become necessary if we intend to have any expected predictive power by which to judge our models.

Most of the time, these computational approaches come in the form of numerical solutions, wherein a set of points that predict the evolution of a system is generated based on the DEs and initial conditions given by the model by working forward from the initial state in small time increments so as to approximate the continuous evolution of variables and their derivatives. The advantages of these solutions come largely in their commonality (and therefore in their reliability). However, these solutions are still hindered by their reliance on a researcher's ability to find the governing differential equations in the first place, which is frequently a not-at-all-straightforward task. Additionally, this approach is often (for more complicated scenarios) computationally expensive.

Enter machine learning and, specifically, physics-informed neural networks. Neural networks hail from the world of computer science, and they've found a number of incredible uses ranging from image recognition to targeted marketing to load forecasting. Until recently, neural networks have been less than useful to physicists, as although they are universal function approximators (and therefore can be made to fit to almost any data they are given), they are prone to generating solutions that, while fitting to the data, fail to resemble anything that obeys physical laws. Physics-informed neural networks seek to solve this problem by embedding physical laws (either as established in differential equations for the system or otherwise) into the learning processes of neural networks via their loss functions. The result is that these neural networks learn to generate solutions that are physically possible and, thus, useful. Additionally, physics-informed neural networks (PINNs) don't always require the discovery of DEs for the system, as there are plenty of other physical laws that can restrict the evolution of these networks. Finally, PINNs are frequently computationally inexpensive when compared with alternative approaches, especially when the problem in question is some complex partial differential equation as is common in certain fields of physics.

In this project, we seek to tackle the modeling of a novel orbital problem involving a small rubber ball rolling around in a large glass bowl. We attempt to do this using analytical, numerical, and machine learning techniques, although the analytic approach largely serves the other two for reasons relating to the existence of solutions.

2 Experimental Procedure

2.1 Generating Data

As previously stated, the explorations of this project surrounded the problem of describing/predicting the motion of a rubber ball as it rolls around a large bowl. As such, two sets of data were generated, each of which corresponds to around seven or eight seconds of positional data of the ball's center relative to the center of the bowl as it rolls. This data was generated by hand by analyzing individual frames of videos of the ball's motion. First, the frames of a given video were extracted using VLC media player. Afterward, the horizontal and vertical (x and y) positions of the ball relative to the bowl's center were found in pixels using Microsoft Paint. This process, although slow, ensured that the positional data gathered was as accurate as it could have been.

In order to take the videos themselves, a great deal of vertical distance was required. As the recording of the ball and bowl is top-down, in order to avoid any optical distortion, the distance from the camera to the experimental setup needed to be maximized. In this case, the ball sat on the 1st floor of the Stephens Science Center, whilst the camera was attached to a railing overhead on the 3rd floor of the building. Below are images of the experimental setup.

The positional data gathered was converted from pixels into centimeters. Raw data tables are found in Appendix A. Graphs of these trials are given below.

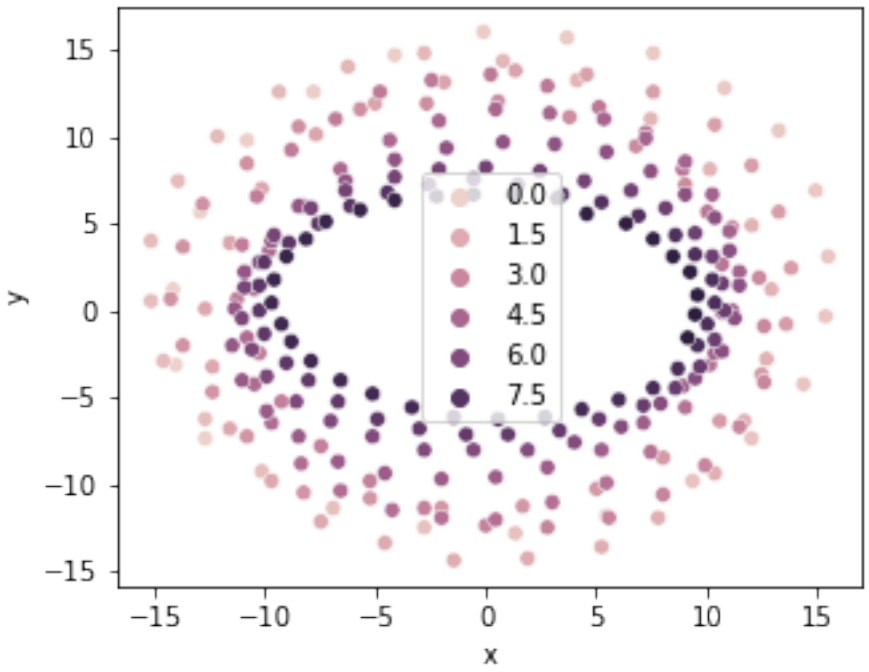

Figure 1: Positional data for the first trial (set 1). Here, x and y are both in centimeters, and the color of the dots indicates time (in seconds).

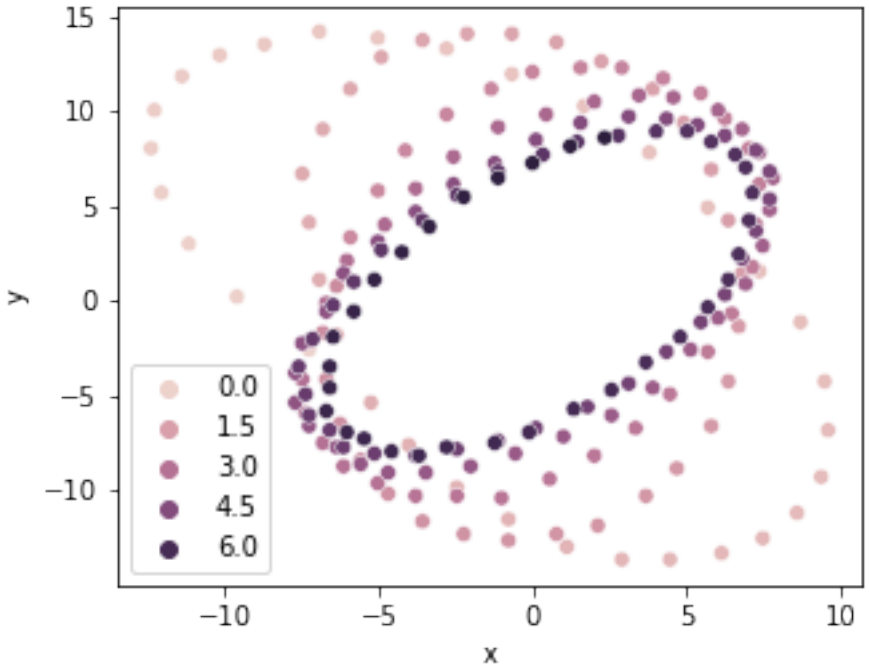

Figure 2: Positional data for the second trial (set 2). Here, x and y are both in centimeters, and the color of the dots indicates time (in seconds).

2.2 Describing the Bowl

In order to do a physical analysis of this scenario, we require knowledge of the shape of the bowl. A mathematical description of the bowl was thus found by fitting various possibilities for the shape of the bowl to data. Three such possibilities for the shape of the bowl were explored: a sphere, a paraboloid, and some other rotated power law shape. Two different methods were used for taking data. The first involved incrementally filling the bowl with water. Here, the volume of water added to the bowl at each step was recorded, as well as the height of the water in the bowl before and after each step. This allowed for the calculation of the cross-sectional area of the bowl at each height and thus (assuming circular cross-sections) the radius at each height. Two such data sets were taken in an attempt to fit the shape of the bowl to a sphere. The graphs, showing both the data and the sphere of best fit, are below.

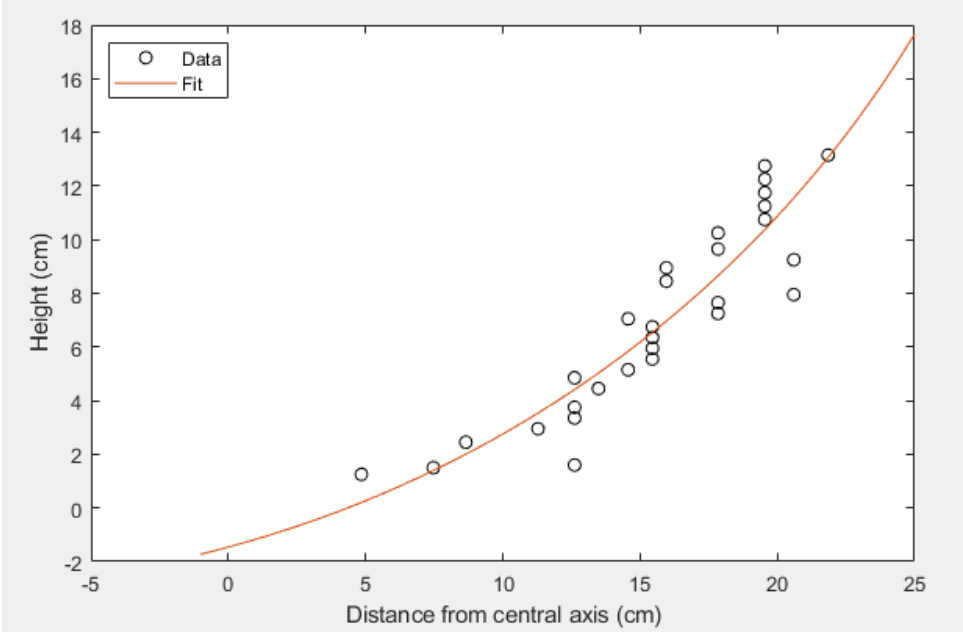

Figure 3: Shape data of the bowl fit to a sphere. Data from the first round of using the water method. Here, the circle of best fit had radius 42.07 cm, and the RMSE was 1.41 cm.

After taking the first set of data (above), a second set was taken with more data points to try to account for the noisiness of the data.

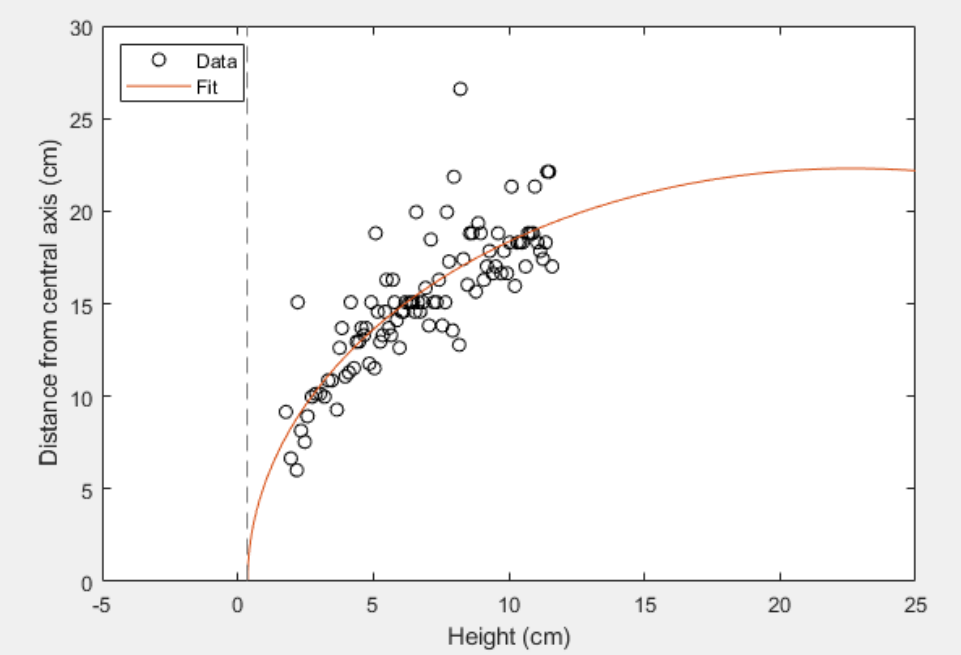

Figure 4: Shape data of the bowl fit to a sphere. Data from the second round of using the water method. Here, the circle of best fit had radius 22.30 cm, and the RMSE was 2.03 cm.

After a second round of noisy data that disagreed with the results of the first by a multiple of around 2, the water method was abandoned. Instead, an approach was used wherein calipers were used to measure the depth of the bowl at various abaxial distances (as measured using a ruler laid over the top of the bowl). Using this method, a single set of data was taken, and the possibility of parabolic and other power law shapes was explored (of the form $z = Cs^n$). The graphs generated are here below.

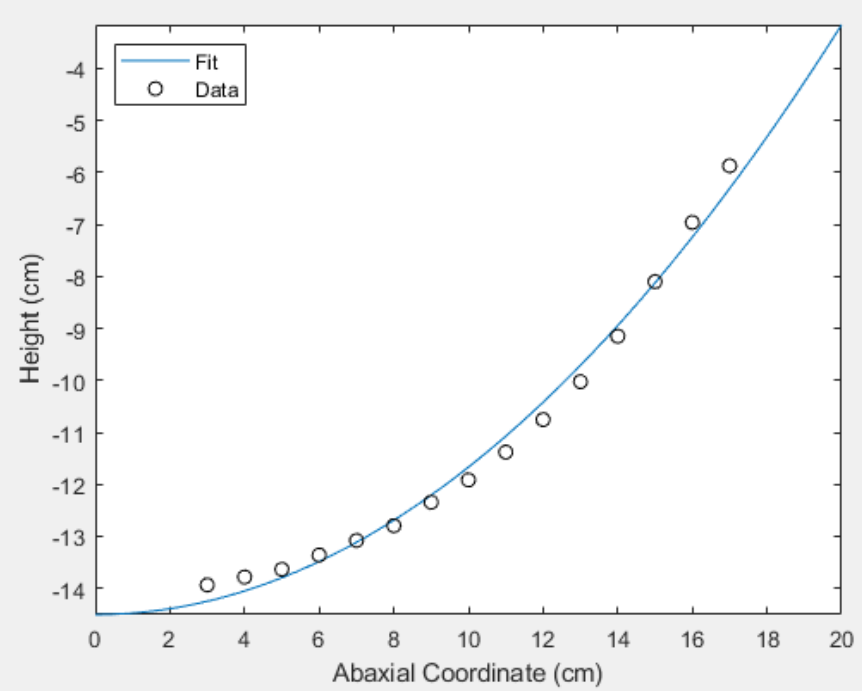

Figure 5: Shape data of the bowl fit to a paraboloid. Data from the caliper method. Here, using the equation $z = Cs^n$, the best fit was with $C = 0.0284$ and $n = 2$. The fit gave RMSE = 0.27 cm.

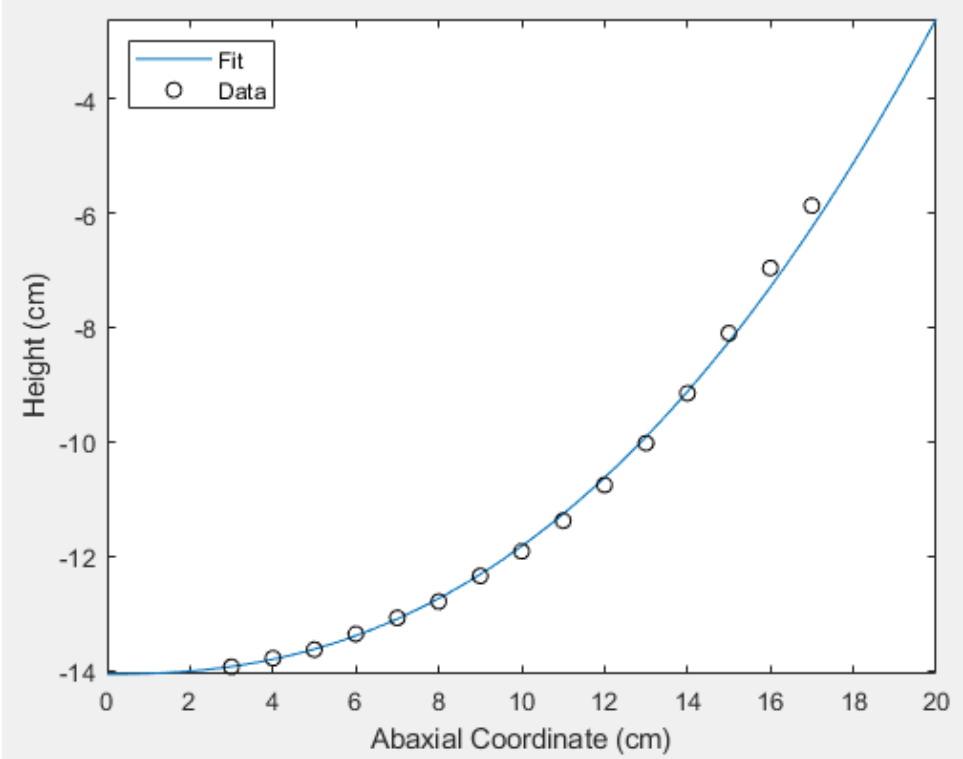

Figure 6: Shape data of the bowl fit to a power law. Data from the caliper method. Here, using the equation $z = Cs^n$, the best fit was with $C = 0.0098$ and $n = 2.36$. The fit gave RMSE = 0.15 cm.

The parabolic and power law fits shown above were both used in the attempts to tackle this problem that follow.

3 Analytic Approach

The first method that we attempted to use to describe the motion of the ball was to, using classical mechanics, find a closed-form solution for the ball's motion.

3.1 Orbital Mechanics

Luckily, orbital problems have been a popular topic of study in the world of classical physics for centuries at this point, and thus we have some existing solutions to problems from which we can draw inspiration. Here, we consider the two-body problem.

The best way to approach the two-body problem is to first move into the center of mass frame of two bodies and consider instead a body with mass equal to the reduced mass of the system, $\mu = \frac{m_1 m_2}{m_1 + m_2}$. Here, we will use polar coordinates, so the abaxial coordinate is r and the azimuthal coordinate is ϕ. If the potential field relevant to our scenario (most frequently gravity) is U, then our Lagrangian is:

$$\mathcal{L} = \frac{1}{2}\mu v^2 - U(r)$$

$$\mathcal{L} = \frac{1}{2}\mu\left(\dot{r}^2 + r^2\dot{\phi}^2\right) - U(r) \tag{1}$$

Then by the Euler-Lagrange equation, we know:

$$\frac{d}{dt}\frac{\partial \mathcal{L}}{\partial \dot{\phi}} = \frac{d}{dt}\left(\mu r^2 \dot{\phi}\right) = 0$$

$$\mu r^2 \dot{\phi} = const = l \tag{2}$$

This is the conservation of angular momentum, l. We also know:

$$\frac{d}{dt}\frac{\partial \mathcal{L}}{\partial \dot{r}} = \frac{\partial \mathcal{L}}{\partial r}$$

$$\mu \ddot{r} = \mu r \dot{\phi}^2 - \frac{dU}{dr}$$

Then by Equation (2):

$$\mu \ddot{r} = \frac{l^2}{\mu r^3} - \frac{dU}{dr}$$

Here, the quantity $\frac{l^2}{\mu r^3}$ can be interpreted as the centrifugal force, a fictional, outward-pointing force that exists in a rotating frame of reference. From the canon of classical mechanics, we know that simple, closed-form solutions to these differential equations exist when U is like gravity (and follows an inverse-square law) or when U obeys Hooke's law (quadratic energy).

3.2 Our Problem

We can apply many of the same techniques listed above to our situation. We move now to cylindrical coordinates, so our abaxial coordinate is s and our azimuthal coordinate is ϕ. Here, we treat our second "body" as one with infinite mass fixed at the center of the bowl. Then the reduced mass is just the mass of the ball, m. To our Lagrangian, we must add a component of rotational kinetic energy. This gives:

$$\mathcal{L} = \frac{1}{2}\mu v^2 + \frac{1}{2} I \omega^2 - mgCs^n$$

Then as $I = \frac{2}{5}mr^2$ for a ball of radius r and as $\omega r = v$, we get:

$$\mathcal{L} = \frac{7}{10} m \left(\dot{s}^2 + s^2 \dot{\phi}^2 \right) - mgCs^n \tag{3}$$

Note that our potential $U = mgCs^n$ is simply gravitational potential energy according to the constants C and n that we found earlier. From this Lagrangian, it is possible to derive the following equations using the Euler-Lagrange equations. Firstly, we have something similar to Equation (2):

$$s^2 \dot{\phi} = const = l \tag{4}$$

Note that here, l is not angular momentum. It is instead a different related, conserved quantity that was selected to be used instead of the angular momentum in order to avoid needing to know the ball's mass. In addition to this equation, we also get the following:

$$\ddot{s} = s\dot{\phi}^2 - \frac{5}{7} gCns^{n-1}$$

Then by Equation (4):

$$\ddot{s} = \frac{l^2}{s^3} - \frac{5}{7} gCns^{n-1} \tag{5}$$

This is the second of the two differential equations that can be extracted.

3.3 Problems with the Approach

There are a number of problems with attempting a purely analytical approach to this problem that thus necessitate some computational elements. Firstly, there is likely no analytic solution for Equation (5) in our case. We know that in the classical orbital problem, using an inverse square force, we have solutions that look like elliptical orbits. We also know that we get similarly simple elliptical orbits from a Hooke's law/quadratic potential (linear force). However, in our case, the power law of best fit has our potential

scaling according to a non-integer power of s that almost certainly does not yield a simple analytic solution.

Secondly, our analytic approach makes heavy use of certain approximations. For one, notice that our Lagrangian, Equation (3), does not include the z-component of velocity. This was done mostly to preserve similarity to the known orbital problem with a known solution, but it is notably more inaccurate the further one gets from the center. Additionally, although our curve of best fit is relatively tight, we still do not have the "true" equation of the bowl

Finally, it is important to note that the use of Lagrangian mechanics in this context may not be physically valid at all. This is because we know that it is possible for the ball to accelerate in the azimuthal direction. Then as we have assumed the rolling condition, we know that there must be some torque acting on the ball that allows it to accelerate in this way. This necessitates an azimuthal force, which would mean that there is a torque acting on the system in the orbital sense. So, angular momentum isn't actually conserved, and for similar reasons, energy also is lost rapidly.

For these reasons, it becomes necessary to use a computational approach.

4 Numerical Approach

The first computational approach attempted was to solve the differential equations we derived using a numerical solver in MATLAB (namely, MATLAB's ode45). In a simplified sense, this solver works by taking small steps forward in time and carefully calculating relevant derivatives and values along the way. Given a differential equation and initial conditions, it can solve the system at incredible speed and ease.

4.1 Simple Solution

We use the numerical solver to solve the DEs we found with no modification. Below are the results of using ode45 to solve the system given by Equations (4) and (5) to model sets 1 and 2. Here, recall that $C = 0.0098$ and $n = 2.36$.

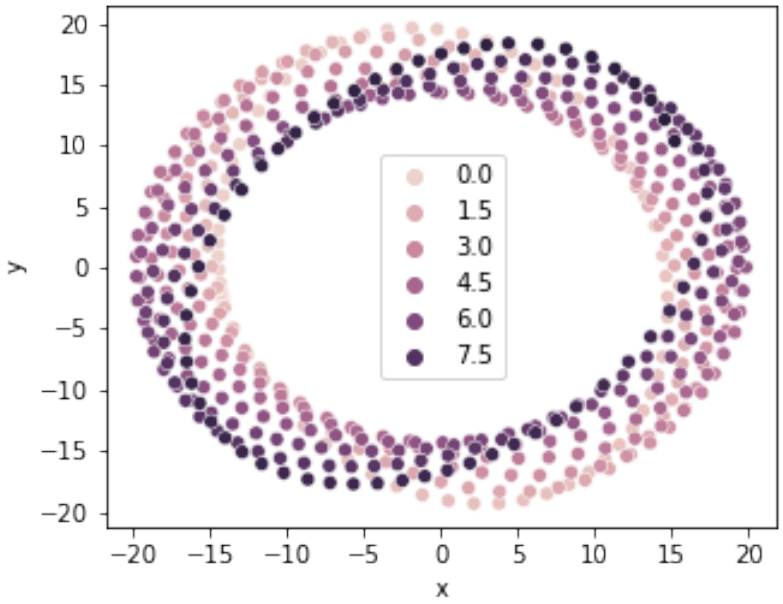

Figure 7: Results of using ode45 to solve our system using initial conditions from set 1 and using the power law fit. Here, x and y are both in centimeters, and the color of the dots indicates time (in seconds). Compare to Figure 1.

Notably, in the above figure, our DE predicts that the ball will reach s values that place it outside of the real bowl.

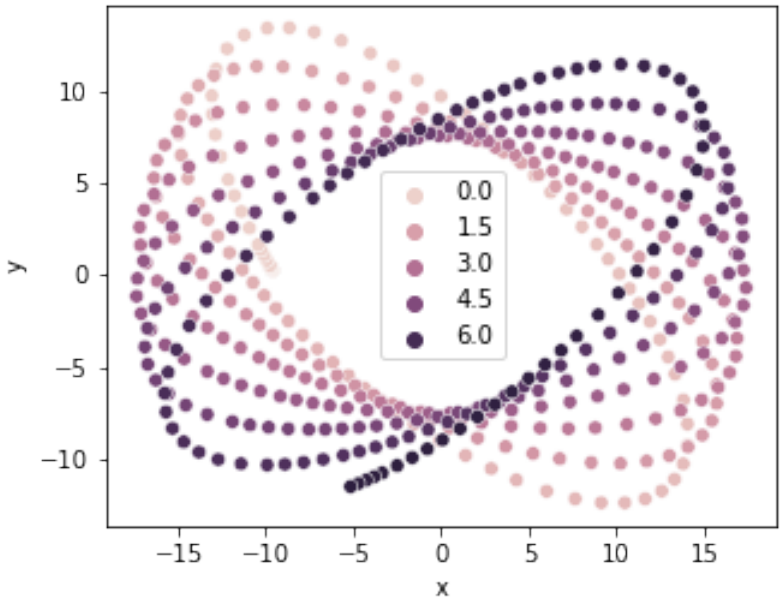

Figure 8: Results of using ode45 to solve our system using initial conditions from set 2 and using the power law fit. Here, x and y are both in centimeters, and the color of the dots indicates time (in seconds). Compare to Figure 2.

A quick comparison between these solutions to the given DEs and the actual data (Figures 1 and 2)

reveals that although the general orbital motion is qualitatively similar, it is notable that in our solutions, the orbit never loses energy. In order to attempt to account for this, we take advantage of the fact that we know angular momentum is not conserved in our specific scenario.

4.2 Accounting for Decay

To account for the loss of energy, we exploit the fact that l is not constant. So, we let $l = s^2\dot{\phi}$ be a function of time by assuming that it is linear and considering the line (in time) that connects the initial value of l with the final value of l as taken from our given data. This function of time is what replaces l in Equations (4) and (5). These are the results of making that adjustment and then solving using MATLAB:

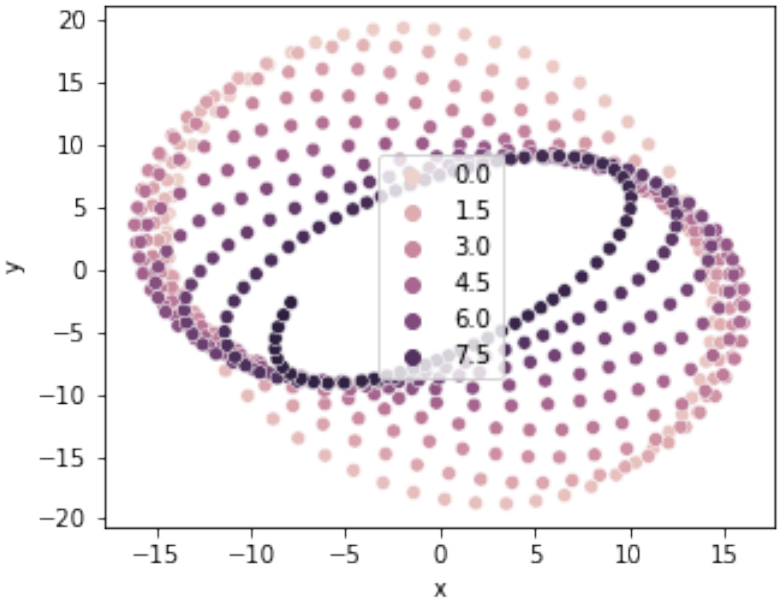

Figure 9: Results of using ode45 to solve our system using initial conditions from set 1 and using the power law fit and assuming that l decays linearly. Here, x and y are both in centimeters, and the color of the dots indicates time (in seconds). Compare to Figure 1.

Again, in the above figure, our DE predicts that the ball will reach s values that place it outside of the real bowl.

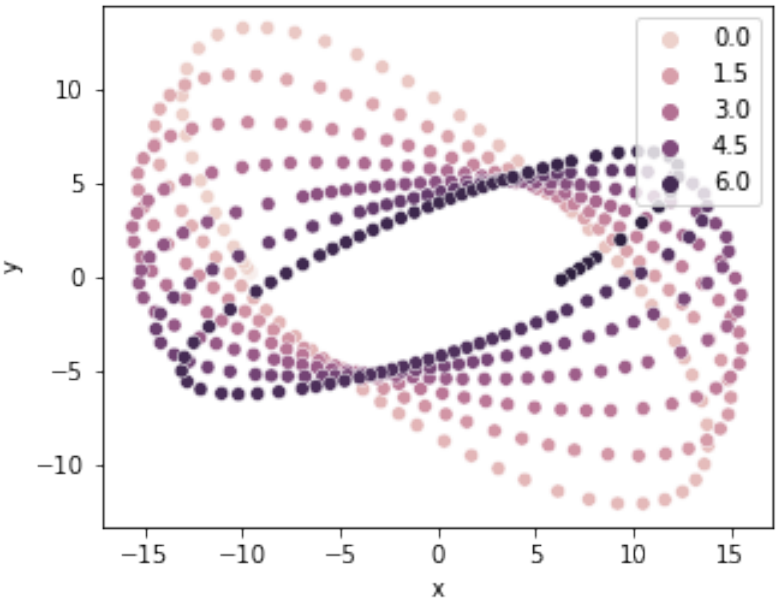

Figure 10: Results of using ode45 to solve our system using initial conditions from set 2 and using the power law fit and assuming that l decays linearly. Here, x and y are both in centimeters, and the color of the dots indicates time (in seconds). Compare to Figure 2.

Having made this adjustment, it appears that our numerically calculated paths now lose energy somewhat similarly to the actual data. However, it now becomes apparent that another major difference between the actual data and the solutions we find with ode45 is that our calculated orbits process, whilst our actual orbits (Figures 1 and 2) do not. Note that set 2 may appear to process at first, but later in its orbit, it locks into a singular elliptical orientation. The lack of procession in an orbit like this is also commonly seen in orbits where the potential energy follows Hooke's law.

4.3 Using Paraboloid Fit

In order to try to further imitate the non-processing orbit that we see in both of our sets of data, we now use the parabolic fit discussed previously (with $C = 0.0284$ and $n = 2$) to solve Equations (4) and (5) numerically. Note that we are still creating artificial loss of energy by modeling l as a function of time. The following are the results for both sets of data. The paths generated appear in Appendix B.

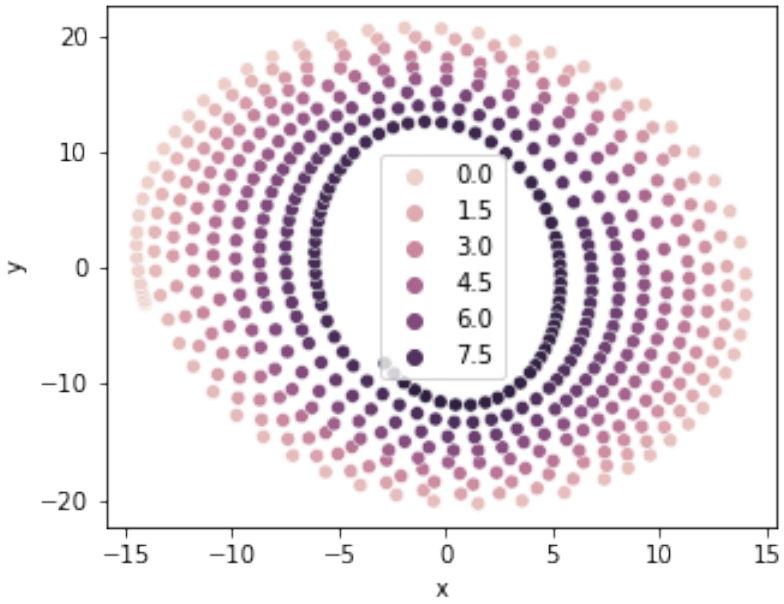

Figure 11: Results of using ode45 to solve our system using initial conditions from set 1 and using the parabolic fit and assuming that l decays linearly. Here, x and y are both in centimeters, and the color of the dots indicates time (in seconds). Compare to Figure 1.

In the above figure, our DE predicts that the ball will reach s values that place it outside of the real bowl.

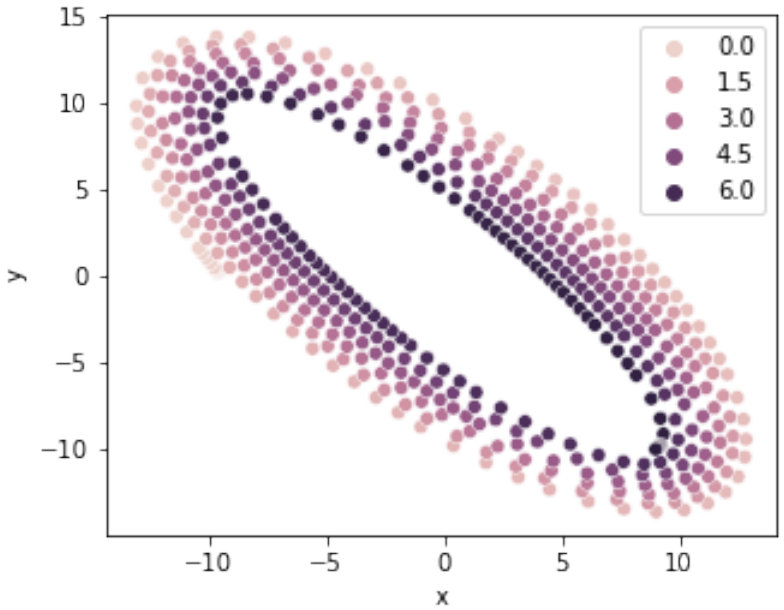

Figure 12: Results of using ode45 to solve our system using initial conditions from set 2 and using the parabolic fit and assuming that l decays linearly. Here, x and y are both in centimeters, and the color of the dots indicates time (in seconds). Compare to Figure 2.

These are the final solutions as produced using an ODE solver for this project. Overall, the ODE solver

managed to imitate many qualitative features, but it still has many suspect flaws (such as the insistence that the first set of data should have resulted in the ball flying out of the bowl). The general shape of the orbit improved significantly for set 1 after assuming a parabolic bowl, but the opposite is true for set 2. We investigate this further by comparing the set 2 data to what is predicted here specifically for only the data points prior to 1.5 seconds:

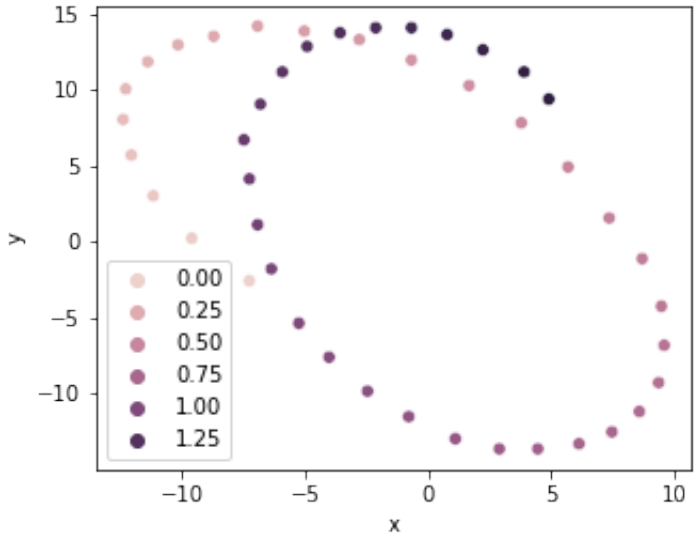

Figure 13: Data from set 2 prior to 1.5 seconds. Here, x and y are both in centimeters, and the color of the dots indicates time (in seconds).

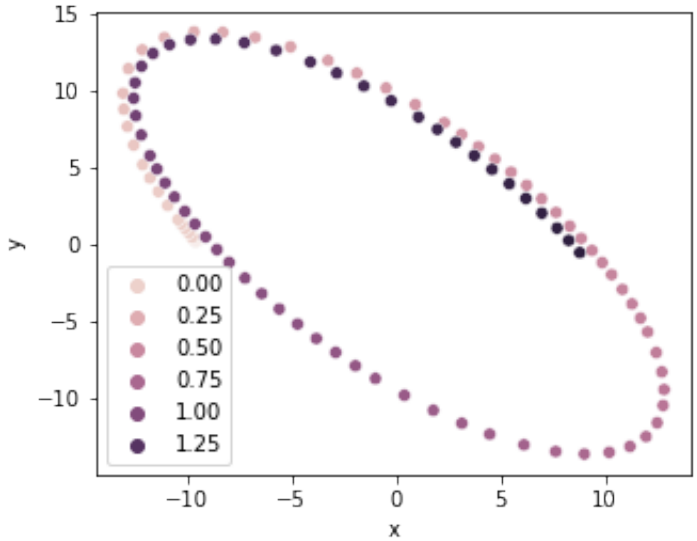

Figure 14: Results prior to 1.5 seconds of using ode45 to solve our system using initial conditions from set 2 and using the parabolic fit and assuming that l decays linearly. Here, x and y are both in centimeters, and the color of the dots indicates time (in seconds). Compare to Figure 13.

From the above two graphs, it becomes clear that prior to around 0.7 seconds or so, our numerical solution manages to find a solution that is, relatively speaking, qualitatively similar to the actual data. At some point in the 3rd quadrant of the original data plot (Figure 13), our ball appears to shift off-course,

taking a hard right turn so to speak. This may be an indication of a slip in the ball (meaning that the ball did not obey the rolling condition for a short time). The astonishing similarity in these two graphs prior to 1.5 seconds can be further highlighted by observing the graphs of x and y over time:

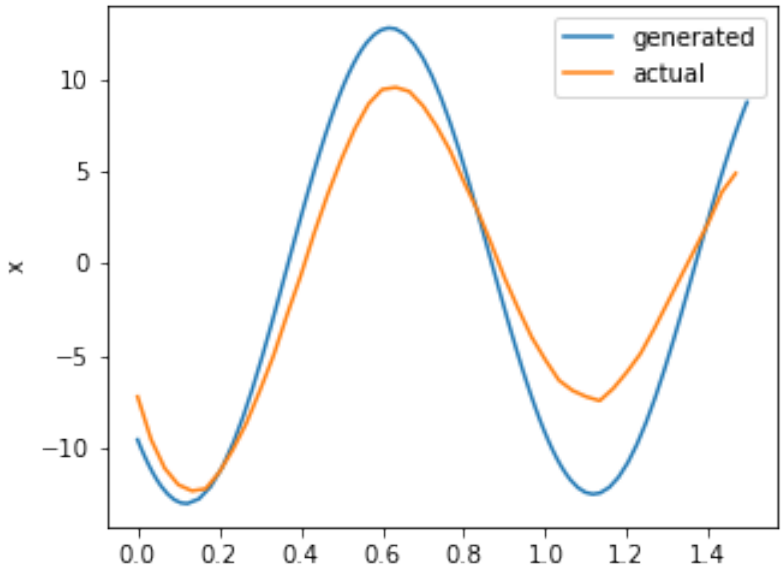

Figure 15: Comparing the y positional data between set 2 and the parabolic numerical solution to set 2 prior to 1.5 seconds. Here, y is in cm.

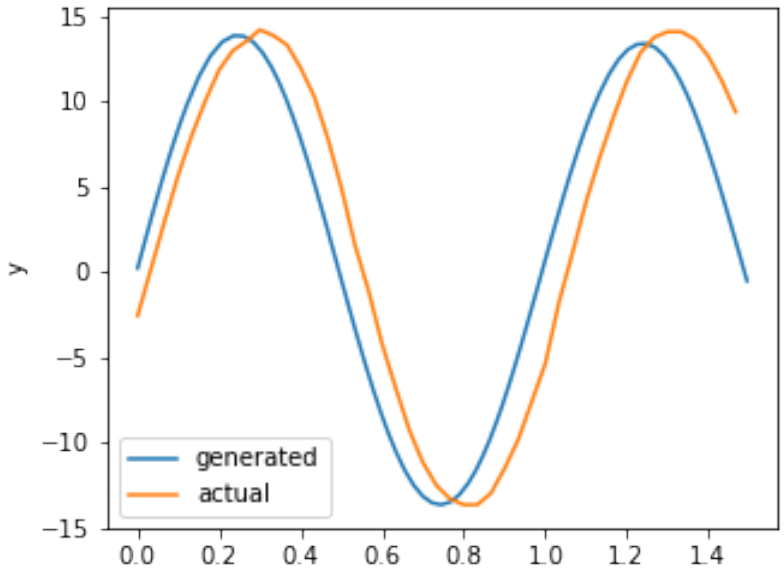

Figure 16: Comparing the x positional data between set 2 and the parabolic numerical solution to set 2 prior to 1.5 seconds. Here, x is in cm.

Notably, it appears that the initial positions of these graphs do not agree with each other. This is simply due to a small shift in the time coordinate data in the numerically generated data that appears as a result

of computing derivatives using centered differences and discarding the resulting missing values. From the above graphs, we see further just how accurate our parabolic, energy-dissipating model was for the early data points of set 2. This would be worth exploring further in future projects.

5 Machine Learning Approach

Aside from numerical approaches, it is possible to approach physical situations such as this one using machine learning techniques. In particular, certain varieties of neural network can be rather useful.

5.1 Background on Neural Networks

Neural networks are highly adaptive, highly versatile universal function approximators that can be used for both regression and classification tasks. Due to their high performance and immense flexibility, neural networks have found applications in image recognition, speech recognition, medical diagnostics, and many other complex realms. Inspired by the human brain, these neural networks are deeply interconnected webs of perceptrons, which are based on neurons, that work together to classify or quantify the data given to them. Consider the following diagram of a perceptron:

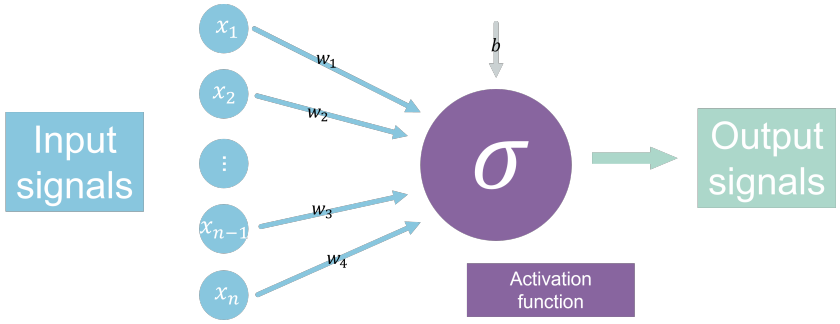

Figure 17: Perceptron schematic. Inputs are taken in with weights applied, and the are then transformed using an activation function to produce an output signal.

As illustrated, an individual perceptron takes in many inputs (and a bias term b) and sums them according to their weights. The result is then passed into an activation function to produce an output signal. Common activation functions include the following:

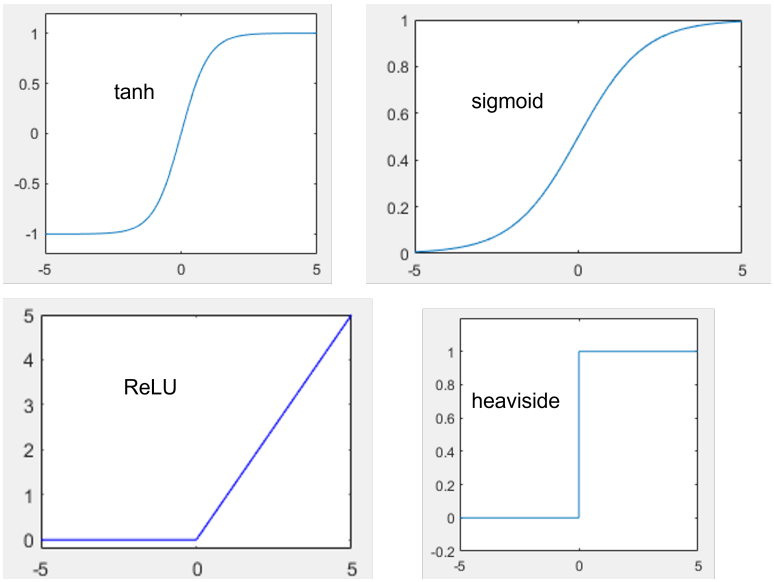

Figure 18: Various activation functions typically used in a perceptron.

In a neural network, multiple layers of these perceptrons are strung together to create an incredibly complex function whose outputs are governed by the weights and biases attached to each perceptron's inputs:

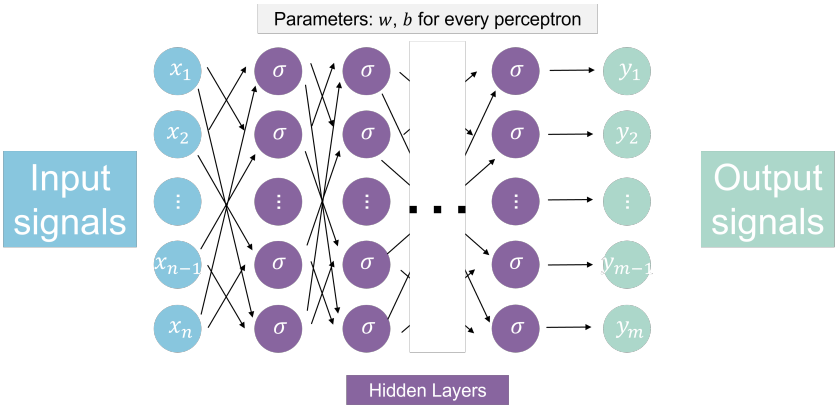

Figure 19: Neural network formed by stringing together multiple layers of individual perceptrons.

These weights and biases are adjusted through an optimization process not unlike typical curve fitting so as to minimize the error in the neural network's predictions for given sets of inputs. The result is a highly complex tool that can approximate any given function given enough time and the right architecture.

5.2 Physics-Informed Neural Networks

Physics-informed neural networks (PINNs) seek to produce solutions to physical situations that obey physical laws. When a neural network is given, for example, positional data of an object whose motion they are being trained to describe, it is almost always capable of finding weights and biases that lead to outputs that match the data given. However, this does not always guarantee that the function produced obeys physical laws. PINNs seek to fix this by embedding physical laws into their loss functions. Consider the following generic ODE:

$$\frac{d}{dt}y = f(y,t)$$

This can be transformed into a loss function of the form:

$$L = \frac{d}{dt}y - f(y,t)$$

This loss function can be added to the typical loss function used to make a neural network match training data. By minimizing this loss function alongside the typical loss functions, the neural network automatically solves the ODE, as when $L = 0$, we have solved our given ODE. This relies, of course, on the inherent ability of neural networks to quickly produce derivatives of their own outputs with respect to their inputs known as autodifferentiation.

Other loss functions can be created much like the one above to encode initial conditions and boundary conditions. By adding all of these loss functions together with the loss function that measures conformity to the data, we can train a neural network such that it both matches the data closely and obeys known physical laws.

5.3 The PINN Approach

Physics-informed neural networks were the last method of modeling our scenario explored in this project. They were implemented using PyTorch. The network architecture initially used was one that accepted one input (time), had three hidden layers, and produced 2 outputs (s and $\dot{s}$). The hidden layers had linear, sigmoid, and linear activation functions in that order.

The first attempt to describe the data involved giving the neural network only two pieces of information (via its loss function): the initial values of s and $\dot{s}$ and the DE described in Equation (5). Unfortunately, this attempt failed, as it produced NaN values. This is likely due to failures in numeric precision during the autodifferentiation step. Upon initiation, a neural network is essentially a mostly-random function. Thus, it is possible for the first version of a neural network to say that s is small or even zero. This breaks the autodifferentiation, as $\ddot{s}$ depends on $\frac{1}{s^3}$, which gets very large when s is small.

In order to remedy this, fail-safes were implemented in the form of functions that replaced NaNs and infinite values with zeros and large numbers respectively. Additionally, more information was given to the neural network in the form of more data points (consisting of s and $\dot{s}$ at given times) aside from just the initial conditions. This still failed to converge and frequently, in training, would produce NaNs all the same.

The final attempt to use PINNs to imitate our data used even more data points and a simplified DE that assumes a Hooke's law potential well. This PINNs produced four outputs (x, y, $\dot{x}$, and $\dot{y}$) according to the differential equations $\ddot{x} = -2Cx$ and $\ddot{y} = -2Cy$ (here, $C = 0.0284$ according to our prior parabolic fit). After some additional tweaking to the learning rate of the neural network, eventually an output was produced. The x and y values as predicted by this network using data from set 1 (Figure 1) are shown below. The data appears in Appendix C.

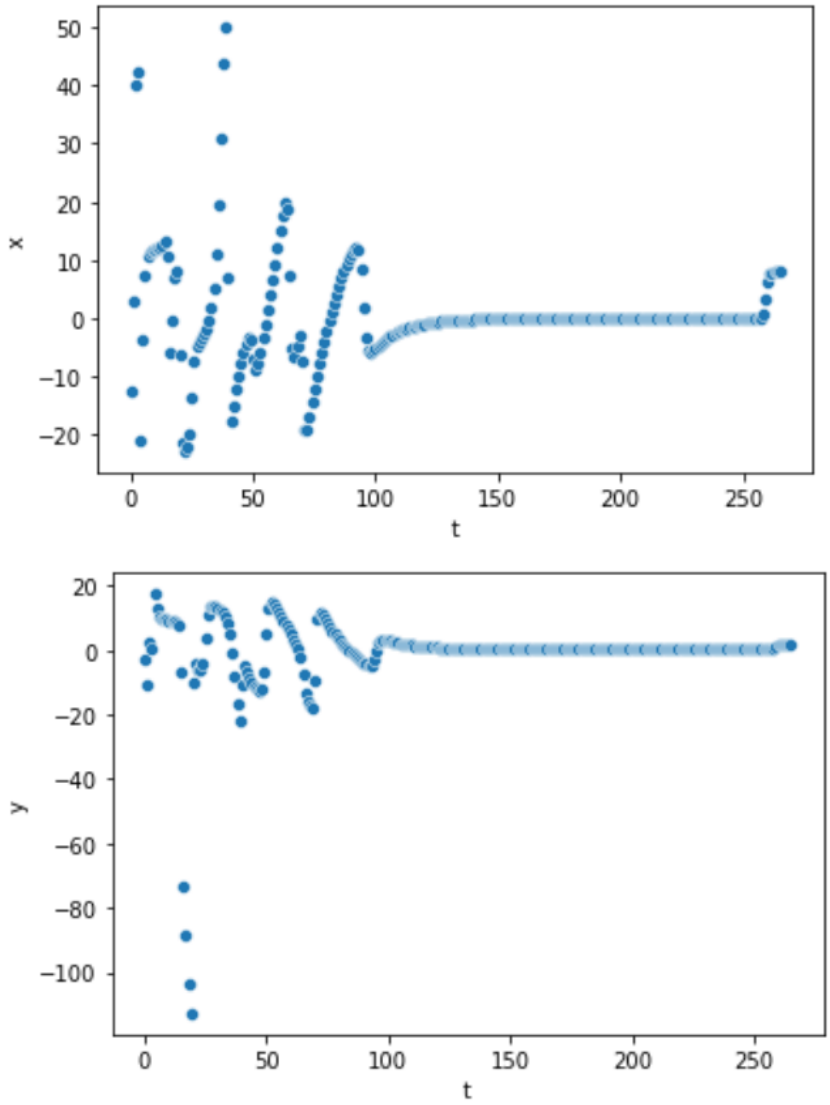

Figure 20: Motion predicted by a PINN using a Hooke's law potential well and true data points. Here, t is in frames ($\frac{1}{30}$ seconds) and x and y are in cm.

Although the PINN managed to produce something similar to oscillatory motion (prior to 100 frames), it is clear that this is nothing similar to the motion observed in reality. It is suspected that this is due to the limited amount of time for which the neural network was allowed to train.

6 Conclusion

In the course of attempting to describe the motion in our system (consisting of a rubber ball rolling around a large bowl), we used three approaches. The first was purely analytic. Using classical techniques that have been used in the two-body problem for centuries, we acquired approximations of differential equations (approximate because of the lack of a z-coordinate and because of our lack of knowledge about the shape of the bowl). This, however, is as far as the analytic approach could take us. No closed-form solution is possible unless we have either Hooke's law energy or an inverse square law force. Thus, we moved on to numerical methods.

In our numerical methods, we used the differential equations that we found analytically to generate

numerical solutions to the path of the ball using the power law fit of the bowl. Our initial attempts were physically sound, but they did not resemble our data in that they never lost energy. This was remedied by assuming that the value of $l = s^2\dot{phi}$ was not constant, but rather linearly decaying over time. The results of this assumption were paths that lost energy in a more plausible-seeming way, but the orbits were still flawed in that they processed, whilst the orbits we observed in the real data did not appear to do so. This was fixed by changing our assumed bowl shape into a parabola using the fit constants that we found prior. Our final numerical solutions are somewhat qualitatively similar to the actual data, but not at all accurate quantitatively.

The final approach used PINNs encoded with the differential equations we discovered as well as some of the real-world data that we collected. For lack of effectiveness, this approach was only used to try to describe the set 1 data. After failing to find solutions for the power law fit of the bowl, the PINN was shifted to instead solve what boils down to a harmonic oscillator in independent coordinates x and y. Whilst the data it produced could be argued to have some of the qualities associated with the expected elliptical orbit, they were still far off the mark.

The best opportunities for improvement on this work are in the analytic and PINN-based areas. A more detailed physical analysis of the scenario at hand could yield more accurate DEs that would then lead to more accurate numeric solutions as well as more accurate PINN-based solutions. The PINNs themselves could greatly benefit from improved network architecture and longer training times. Additionally, more work should be done to find how to work around the problem of values that cannot be handled by the typical float64 number system used in computers.

7 Appendix A: Raw Data

The following is the data from set 1 (Figure 1).

Table 1: Set 1 Positional Data

t (s)	x (cm)	y (cm)	t (s)	x (cm)	y (cm)	t (s)	x (cm)	y (cm)	t (s)	x (cm)	y (cm)	t (s)	x (cm)	y (cm)
0.00	-12.72	-7.36	2.00	12.05	8.37	4.00	3.01	-11.04	6.00	-2.79	-8.03	8.00	2.68	-6.14
0.03	-14.06	-3.12	2.03	13.27	5.69	4.03	0.45	-12.05	6.03	-5.13	-7.25	8.03	0.56	-6.25
0.07	-14.17	1.23	2.07	13.83	2.45	4.07	-2.01	-11.94	6.07	-7.03	-6.36	8.07	-1.45	-6.14
0.10	-12.94	5.69	2.10	13.61	-0.78	4.10	-4.24	-11.49	6.10	-8.59	-5.24	8.10	-3.35	-5.58
0.13	-10.82	9.82	2.13	12.49	-3.68	4.13	-6.58	-10.37	6.13	-9.93	-3.79	8.13	-5.13	-4.80
0.17	-7.81	12.60	2.17	10.60	-6.36	4.17	-8.37	-8.81	6.17	-10.60	-2.23	8.17	-6.58	-4.02
0.20	-4.13	14.72	2.20	8.03	-8.48	4.20	-9.70	-6.47	6.20	-11.04	-0.45	8.20	-7.92	-2.90
0.23	-0.11	16.06	2.23	5.02	-10.26	4.23	-10.49	-4.24	6.23	-10.93	1.34	8.23	-8.81	-1.78
0.27	3.68	15.73	2.27	1.67	-11.27	4.27	-10.82	-1.56	6.27	-10.26	2.79	8.27	-9.26	-0.78
0.30	7.59	14.84	2.30	-2.01	-11.38	4.30	-10.49	1.23	6.30	-9.59	4.35	8.30	-9.70	0.45
0.33	10.82	12.83	2.33	-5.24	-10.82	4.33	-9.82	3.46	6.33	-7.92	5.91	8.33	-9.59	1.78
0.37	13.27	10.37	2.37	-8.25	-10.49	4.37	-8.25	6.02	6.37	-6.36	6.92	8.37	-9.04	3.12
0.40	14.95	6.92	2.40	-10.82	-7.25	4.40	-6.58	8.14	6.40	-4.13	7.70	8.40	-8.14	4.13
0.43	15.51	3.12	2.43	-12.38	-4.69	4.43	-4.35	9.82	6.43	-2.12	8.14	8.43	-7.25	5.13
0.47	15.39	-0.33	2.47	-13.72	-2.01	4.47	-2.12	10.93	6.47	0.00	8.25	8.47	-5.69	5.80
0.50	14.39	-4.24	2.50	-14.28	0.67	4.50	0.45	11.60	6.50	2.45	8.03	8.50	-4.13	6.36
0.53	12.05	-7.36	2.53	-13.72	3.68	4.53	2.90	11.38	6.53	4.46	7.47	8.53	-2.23	6.58
0.57	9.37	-9.82	2.57	-12.83	6.14	4.57	5.35	11.04	6.57	6.58	6.92	8.57	-0.56	6.69
0.60	5.47	-11.82	2.60	-10.82	8.48	4.60	7.25	9.93	6.60	8.14	5.91	8.60	1.23	6.69
0.63	1.34	-12.83	2.63	-8.48	10.60	4.63	9.04	8.59	6.63	9.48	4.46	8.63	3.23	6.47
0.67	-2.79	-12.49	2.67	-5.69	11.60	4.67	10.26	6.69	6.67	10.26	3.12	8.67	4.57	5.58
0.70	-6.92	-11.38	2.70	-2.68	11.94	4.70	11.04	4.57	6.70	10.71	1.56	8.70	6.36	5.02
0.73	-10.15	-9.26	2.73	0.56	12.05	4.73	11.49	2.23	6.73	10.82	0.00	8.73	7.59	4.13
0.77	-12.72	-6.25	2.77	3.79	11.15	4.77	11.15	0.00	6.77	10.37	-1.67	8.77	8.48	3.12
0.80	-14.61	-2.90	2.80	6.80	9.48	4.80	10.37	-2.45	6.80	9.70	-3.23	8.80	9.26	2.23
0.83	-15.17	0.56	2.83	9.04	7.25	4.83	8.92	-4.35	6.83	8.59	-4.46	8.83	9.59	0.89
0.87	-15.17	4.02	2.87	11.15	4.80	4.87	7.14	-6.47	6.87	7.14	-5.47	8.87	9.48	-0.22
0.90	-13.94	7.47	2.90	12.38	1.90	4.90	5.24	-8.03	6.90	5.13	-6.25	8.90	9.15	-1.56
0.93	-12.16	10.04	2.93	12.60	-0.89	4.93	2.79	-9.04	6.93	3.35	-6.92			
0.97	-9.37	12.60	2.97	12.60	-4.13	4.97	0.45	-9.59	6.97	1.00	-7.14			
1.00	-6.25	14.06	3.00	11.49	-6.69	5.00	-2.01	-9.70	7.00	-0.89	-7.14			
1.03	-2.79	14.84	3.03	9.93	-8.92	5.03	-4.57	-9.37	7.03	-3.01	-6.80			
1.07	0.78	14.39	3.07	8.03	-10.60	5.07	-6.69	-8.70	7.07	-4.91	-6.25			
1.10	4.13	13.27	3.10	5.58	-11.94	5.10	-8.48	-7.25	7.10	-6.69	-5.24			
1.13	7.47	11.04	3.13	2.79	-12.49	5.13	-9.93	-5.80	7.13	-8.03	-4.02			
1.17	10.15	8.14	3.17	0.00	-12.38	5.17	-11.04	-4.02	7.17	-9.04	-3.01			
1.20	12.05	4.91	3.20	-2.79	-11.38	5.20	-11.49	-2.01	7.20	-10.04	-1.34			
1.23	12.94	1.23	3.23	-5.24	-9.82	5.23	-11.38	0.11	7.23	-10.26	0.00			
1.27	12.72	-2.79	3.27	-7.47	-7.81	5.27	-10.93	2.23	7.27	-10.26	1.45			
1.30	11.71	-6.36	3.30	-9.26	-5.24	5.30	-9.70	4.02	7.30	-10.04	2.79			
1.33	10.37	-9.37	3.33	-10.26	-2.45	5.33	-8.48	6.02	7.33	-8.92	3.90			
1.37	7.81	-11.94	3.37	-11.27	0.67	5.37	-6.36	7.47	7.37	-7.59	5.02			
1.40	5.24	-13.61	3.40	-11.04	3.79	5.40	-4.13	8.70	7.40	-6.14	6.02			
1.43	1.90	-14.28	3.43	-10.37	6.58	5.43	-1.78	9.37	7.43	-4.46	6.80			
1.47	-1.45	-14.39	3.47	-8.81	9.26	5.47	0.78	9.70	7.47	-2.57	7.25			
1.50	-4.57	-13.39	3.50	-6.80	11.04	5.50	3.12	9.59	7.50	-0.56	7.59			
1.53	-7.47	-12.16	3.53	-4.80	12.60	5.53	5.47	9.15	7.53	1.45	7.25			
1.57	-9.70	-9.82	3.57	-2.45	13.27	5.57	7.47	8.03	7.57	3.46	6.69			
1.60	-11.60	-6.80	3.60	0.22	13.61	5.60	9.04	6.69	7.60	5.24	6.25			
1.63	-12.38	-3.23	3.63	2.79	12.94	5.63	10.37	5.35	7.63	6.92	5.47			
1.67	-12.72	0.11	3.67	5.13	11.71	5.67	11.04	3.46	7.67	8.59	4.35			
1.70	-11.60	3.90	3.70	7.25	10.26	5.70	11.49	1.45	7.70	9.48	3.23			
1.73	-10.15	7.03	3.73	8.92	8.14	5.73	11.27	-0.45	7.73	10.26	1.78			
1.77	-7.70	10.15	3.77	10.04	5.69	5.77	10.71	-2.34	7.77	10.37	0.45			
1.80	-5.02	11.94	3.80	10.71	2.68	5.80	9.48	-3.90	7.80	10.04	-0.78			
1.83	-1.90	13.16	3.83	10.71	-0.11	5.83	7.92	-5.35	7.83	9.59	-2.01			
1.87	1.34	13.83	3.87	10.15	-3.12	5.87	6.14	-6.69	7.87	8.70	-3.35			
1.90	4.57	13.61	3.90	9.04	-5.58	5.90	4.02	-7.59	7.90	7.59	-4.46			
1.93	7.59	12.60	3.93	7.47	-8.14	5.93	1.90	-8.03	7.93	6.02	-5.13			
1.97	10.37	10.71	3.97	5.47	-9.93	5.97	-0.56	-8.03	7.97	4.35	-5.69			

The following is the data from set 2 (Figure 2).

Table 2: Set 2 Positional Data

t (s)	x (cm)	y (cm)	t (s)	x (cm)	y (cm)	t (s)	x (cm)	y (cm)	t (s)	x (cm)	y (cm)
0.00	-7.25	-2.57	2.00	-6.25	-6.47	4.00	-5.58	-8.59	6.00	2.57	-4.69
0.03	-9.59	0.22	2.03	-6.69	-4.13	4.03	-6.36	-7.70	6.03	1.34	-5.69
0.07	-11.15	3.01	2.07	-6.80	-1.67	4.07	-7.25	-6.58	6.07	-0.11	-6.92
0.10	-12.05	5.69	2.10	-6.36	0.78	4.10	-7.70	-5.35	6.10	-1.23	-7.47
0.13	-12.38	8.03	2.13	-5.91	3.35	4.13	-7.70	-3.79	6.13	-2.79	-7.70
0.17	-12.27	10.04	2.17	-5.02	5.80	4.17	-7.47	-2.23	6.17	-3.68	-8.14
0.20	-11.38	11.82	2.20	-4.13	7.92	4.20	-6.69	-0.56	6.20	-4.57	-7.92
0.23	-10.15	12.94	2.23	-2.79	9.82	4.23	-6.14	1.45	6.23	-5.47	-7.25
0.27	-8.70	13.50	2.27	-1.34	11.15	4.27	-5.02	3.12	6.27	-6.02	-6.92
0.30	-6.92	14.17	2.30	0.00	12.05	4.30	-3.79	4.69	6.30	-6.69	-5.80
0.33	-5.02	13.83	2.33	1.56	12.27	4.33	-2.57	6.14	6.33	-6.58	-4.57
0.37	-2.79	13.27	2.37	2.90	12.27	4.37	-1.23	7.25	6.37	-6.58	-3.46
0.40	-0.67	11.94	2.40	4.24	11.71	4.40	0.11	8.48	6.40	-6.47	-1.90
0.43	1.67	10.26	2.43	5.47	10.93	4.43	1.56	9.37	6.43	-5.80	-0.56
0.47	3.79	7.81	2.47	6.25	9.59	4.47	3.12	9.70	6.47	-5.13	1.12
0.50	5.69	4.91	2.50	7.03	8.03	4.50	4.35	9.59	6.50	-4.24	2.57
0.53	7.36	1.56	2.53	7.36	6.14	4.53	5.35	9.26	6.53	-3.35	3.90
0.57	8.70	-1.12	2.57	7.25	4.02	4.57	6.25	8.70	6.57	-2.23	5.47
0.60	9.48	-4.24	2.60	7.14	1.78	4.60	7.25	7.92	6.60	-1.12	6.47
0.63	9.59	-6.80	2.63	6.47	-0.67	4.63	7.70	6.80	6.63	0.00	7.25
0.67	9.37	-9.26	2.67	5.69	-2.68	4.67	7.70	5.35	6.67	1.23	8.14
0.70	8.59	-11.15	2.70	4.46	-4.91	4.70	7.25	3.68	6.70	2.34	8.59
0.73	7.47	-12.49	2.73	3.35	-6.69	4.73	6.80	2.23			
0.77	6.14	-13.27	2.77	2.01	-8.14	4.77	6.25	0.33			
0.80	4.46	-13.61	2.80	0.56	-9.37	4.80	5.47	-1.12			
0.83	2.90	-13.61	2.83	-1.00	-10.37	4.83	4.35	-2.68			
0.87	1.12	-12.94	2.87	-2.45	-10.26	4.87	3.12	-4.35			
0.90	-0.78	-11.49	2.90	-3.79	-10.26	4.90	1.78	-5.58			
0.93	-2.45	-9.82	2.93	-5.02	-9.59	4.93	0.11	-6.69			
0.97	-4.02	-7.59	2.97	-6.14	-8.70	4.97	-1.12	-7.36			
1.00	-5.24	-5.35	3.00	-6.80	-7.47	5.00	-2.45	-7.81			
1.03	-6.36	-1.78	3.03	-7.36	-5.91	5.03	-3.79	-8.14			
1.07	-6.92	1.12	3.07	-7.47	-4.13	5.07	-5.13	-8.03			
1.10	-7.25	4.13	3.10	-7.25	-2.12	5.10	-6.14	-7.70			
1.13	-7.47	6.69	3.13	-6.69	-0.11	5.13	-6.58	-6.80			
1.17	-6.80	9.04	3.17	-6.02	2.12	5.17	-7.25	-6.02			
1.20	-5.91	11.15	3.20	-4.80	4.02	5.20	-7.36	-4.91			
1.23	-4.91	12.83	3.23	-3.79	5.91	5.23	-7.59	-3.46			
1.27	-3.57	13.72	3.27	-2.57	7.59	5.27	-7.14	-2.01			
1.30	-2.12	14.06	3.30	-1.12	9.15	5.30	-6.47	-0.22			
1.33	-0.67	14.06	3.33	0.45	9.82	5.33	-5.80	1.00			
1.37	0.78	13.61	3.37	2.01	10.49	5.37	-4.91	2.68			
1.40	2.23	12.60	3.40	3.46	10.82	5.40	-3.57	4.24			
1.43	3.90	11.15	3.43	4.57	10.71	5.43	-2.45	5.58			
1.47	4.91	9.37	3.47	6.02	10.04	5.47	-1.12	6.80			
1.50	5.80	6.92	3.50	6.80	9.04	5.50	0.33	7.70			
1.53	6.36	4.24	3.53	7.36	7.81	5.53	1.45	8.37			
1.57	6.80	1.45	3.57	7.81	6.47	5.57	2.79	8.70			
1.60	6.69	-1.34	3.60	7.70	4.80	5.60	4.02	8.92			
1.63	6.36	-4.24	3.63	7.47	2.90	5.63	5.02	8.92			
1.67	5.80	-6.58	3.67	6.92	0.89	5.67	5.80	8.37			
1.70	4.69	-8.81	3.70	6.02	-0.89	5.70	6.58	7.70			
1.73	3.68	-10.26	3.73	5.13	-2.57	5.73	6.92	7.03			
1.77	2.12	-11.82	3.77	3.90	-4.57	5.77	7.14	5.69			
1.80	0.78	-12.27	3.80	2.57	-6.02	5.80	7.03	4.24			
1.83	-0.78	-12.60	3.83	1.00	-7.14	5.83	6.69	2.45			
1.87	-2.23	-12.27	3.87	-0.56	-8.03	5.87	6.36	1.12			
1.90	-3.57	-11.60	3.90	-2.01	-8.70	5.90	5.69	-0.33			
1.93	-4.69	-10.15	3.93	-3.46	-9.04	5.93	4.80	-1.90			
1.97	-5.58	-8.37	3.97	-4.69	-9.04	5.97	3.68	-3.23			

8 Appendix B: Paraboloidal Numerical Path Data

The following is the path meant to model set 1 shown in Figure 11.

Table 3: Paraboloidal Model of set 1 using MATLAB

t (s)	x (cm)	y (cm)	t (s)	x (cm)	y (cm)	t (s)	x (cm)	y (cm)	t (s)	x (cm)	y (cm)	t (s)	x (cm)	y (cm)
0.00	1.61	0.02	0.87	1.97	-0.57	1.94	1.57	-1.32	3.01	1.32	-2.10	4.06	1.32	-2.86
0.00	1.61	0.02	0.89	1.88	-0.58	1.96	1.49	-1.34	3.03	1.34	-2.12	4.07	1.38	-2.87
0.00	1.61	0.02	0.91	1.79	-0.60	1.98	1.44	-1.36	3.04	1.37	-2.13	4.09	1.43	-2.88
0.00	1.60	0.02	0.93	1.70	-0.61	2.00	1.42	-1.39	3.06	1.42	-2.15	4.10	1.49	-2.89
0.00	1.60	0.02	0.95	1.62	-0.63	2.03	1.43	-1.41	3.07	1.48	-2.16	4.11	1.55	-2.90
0.01	1.60	0.02	0.97	1.57	-0.65	2.04	1.45	-1.42	3.09	1.53	-2.17	4.13	1.62	-2.91
0.01	1.60	0.02	0.98	1.53	-0.66	2.05	1.49	-1.44	3.10	1.59	-2.18	4.14	1.68	-2.92
0.01	1.60	0.01	1.00	1.51	-0.68	2.07	1.53	-1.45	3.11	1.65	-2.19	4.15	1.74	-2.92
0.01	1.60	0.01	1.02	1.51	-0.70	2.08	1.59	-1.46	3.13	1.71	-2.20	4.17	1.79	-2.93
0.02	1.61	0.00	1.03	1.53	-0.71	2.09	1.64	-1.47	3.14	1.77	-2.21	4.19	1.85	-2.94
0.03	1.61	-0.01	1.04	1.56	-0.73	2.11	1.70	-1.48	3.16	1.84	-2.22	4.21	1.90	-2.95
0.04	1.63	-0.02	1.06	1.60	-0.74	2.12	1.77	-1.49	3.17	1.89	-2.23	4.23	1.93	-2.96
0.05	1.65	-0.02	1.07	1.64	-0.75	2.13	1.83	-1.50	3.19	1.94	-2.24	4.25	1.93	-2.97
0.06	1.68	-0.03	1.08	1.69	-0.76	2.15	1.89	-1.51	3.21	2.00	-2.25	4.28	1.91	-2.98
0.07	1.72	-0.04	1.10	1.75	-0.77	2.16	1.95	-1.52	3.23	2.03	-2.26	4.30	1.87	-2.99
0.08	1.76	-0.05	1.11	1.81	-0.78	2.18	2.01	-1.53	3.26	2.03	-2.27	4.32	1.80	-3.00
0.09	1.80	-0.06	1.12	1.87	-0.79	2.20	2.05	-1.54	3.28	2.01	-2.28	4.35	1.71	-3.01
0.11	1.86	-0.07	1.14	1.94	-0.80	2.22	2.11	-1.55	3.30	1.97	-2.29	4.37	1.62	-3.02
0.12	1.92	-0.08	1.15	2.00	-0.81	2.24	2.13	-1.56	3.32	1.91	-2.30	4.39	1.53	-3.04
0.13	1.98	-0.09	1.17	2.06	-0.82	2.27	2.13	-1.57	3.34	1.84	-2.31	4.41	1.43	-3.05
0.15	2.04	-0.10	1.18	2.11	-0.83	2.29	2.09	-1.58	3.36	1.75	-2.32	4.43	1.34	-3.07
0.16	2.11	-0.11	1.20	2.17	-0.84	2.31	2.05	-1.59	3.38	1.66	-2.33	4.45	1.25	-3.09
0.18	2.17	-0.12	1.23	2.21	-0.85	2.33	1.98	-1.60	3.40	1.56	-2.35	4.47	1.19	-3.11
0.19	2.22	-0.13	1.25	2.23	-0.86	2.35	1.90	-1.61	3.42	1.47	-2.36	4.49	1.15	-3.14
0.21	2.26	-0.14	1.27	2.22	-0.87	2.37	1.82	-1.63	3.44	1.39	-2.38	4.52	1.16	-3.16
0.23	2.30	-0.15	1.29	2.20	-0.88	2.39	1.72	-1.64	3.46	1.33	-2.40	4.53	1.18	-3.18
0.25	2.32	-0.16	1.31	2.15	-0.89	2.41	1.63	-1.65	3.47	1.29	-2.41	4.54	1.21	-3.19
0.27	2.31	-0.16	1.33	2.08	-0.90	2.43	1.54	-1.67	3.49	1.27	-2.43	4.55	1.25	-3.20
0.29	2.30	-0.17	1.36	1.99	-0.91	2.45	1.46	-1.69	3.51	1.26	-2.45	4.57	1.30	-3.22
0.31	2.26	-0.18	1.38	1.91	-0.92	2.47	1.42	-1.70	3.52	1.27	-2.46	4.58	1.35	-3.23
0.33	2.21	-0.19	1.39	1.82	-0.94	2.48	1.38	-1.72	3.53	1.30	-2.48	4.59	1.41	-3.24
0.34	2.14	-0.20	1.41	1.73	-0.95	2.50	1.37	-1.74	3.54	1.33	-2.49	4.61	1.47	-3.25
0.36	2.06	-0.22	1.43	1.64	-0.97	2.52	1.37	-1.75	3.56	1.37	-2.50	4.62	1.53	-3.26
0.38	1.97	-0.23	1.45	1.56	-0.99	2.53	1.39	-1.77	3.57	1.42	-2.51	4.63	1.60	-3.26
0.40	1.88	-0.24	1.48	1.50	-1.01	2.55	1.43	-1.79	3.58	1.47	-2.52	4.65	1.66	-3.27
0.42	1.79	-0.26	1.50	1.47	-1.03	2.56	1.48	-1.80	3.60	1.53	-2.53	4.66	1.72	-3.28
0.44	1.71	-0.27	1.52	1.47	-1.05	2.58	1.54	-1.81	3.61	1.58	-2.54	4.68	1.77	-3.29
0.46	1.63	-0.29	1.53	1.48	-1.06	2.59	1.59	-1.82	3.62	1.65	-2.55	4.70	1.83	-3.30
0.48	1.58	-0.31	1.54	1.51	-1.08	2.60	1.65	-1.83	3.64	1.71	-2.56	4.72	1.86	-3.31
0.50	1.56	-0.33	1.56	1.55	-1.09	2.62	1.71	-1.84	3.65	1.77	-2.57	4.75	1.88	-3.32
0.53	1.57	-0.35	1.57	1.60	-1.10	2.63	1.77	-1.85	3.66	1.82	-2.58	4.77	1.87	-3.33
0.54	1.59	-0.37	1.59	1.66	-1.12	2.64	1.84	-1.86	3.68	1.89	-2.59	4.79	1.83	-3.34
0.55	1.62	-0.38	1.60	1.72	-1.13	2.66	1.90	-1.87	3.70	1.94	-2.60	4.81	1.77	-3.35
0.57	1.67	-0.39	1.61	1.78	-1.14	2.68	1.95	-1.88	3.72	1.97	-2.60	4.84	1.70	-3.36
0.58	1.72	-0.41	1.63	1.84	-1.15	2.69	2.00	-1.89	3.74	1.98	-2.61	4.86	1.61	-3.37
0.59	1.78	-0.42	1.64	1.91	-1.15	2.72	2.05	-1.90	3.77	1.97	-2.62	4.88	1.51	-3.38
0.61	1.84	-0.43	1.66	1.97	-1.16	2.74	2.08	-1.91	3.79	1.94	-2.64	4.90	1.41	-3.40
0.62	1.90	-0.44	1.67	2.03	-1.17	2.76	2.08	-1.92	3.82	1.87	-2.65	4.92	1.32	-3.41
0.64	1.96	-0.45	1.69	2.07	-1.18	2.79	2.06	-1.93	3.84	1.78	-2.66	4.94	1.23	-3.43
0.65	2.03	-0.46	1.71	2.13	-1.19	2.81	2.01	-1.94	3.86	1.70	-2.67	4.95	1.17	-3.44
0.67	2.09	-0.47	1.73	2.17	-1.20	2.83	1.95	-1.95	3.88	1.61	-2.68	4.97	1.13	-3.46
0.68	2.15	-0.47	1.75	2.18	-1.21	2.85	1.87	-1.96	3.90	1.52	-2.70	4.98	1.10	-3.48
0.70	2.19	-0.48	1.77	2.17	-1.22	2.87	1.78	-1.97	3.92	1.42	-2.71	5.00	1.09	-3.50
0.72	2.24	-0.49	1.80	2.14	-1.23	2.89	1.69	-1.99	3.94	1.33	-2.73	5.01	1.10	-3.51
0.75	2.27	-0.51	1.82	2.08	-1.24	2.91	1.60	-2.00	3.96	1.26	-2.75	5.03	1.13	-3.53
0.77	2.27	-0.52	1.84	2.01	-1.25	2.93	1.51	-2.02	3.99	1.22	-2.78	5.04	1.17	-3.55
0.79	2.24	-0.53	1.86	1.93	-1.27	2.95	1.43	-2.03	4.01	1.21	-2.80	5.06	1.22	-3.56
0.81	2.19	-0.54	1.88	1.84	-1.28	2.96	1.37	-2.05	4.02	1.22	-2.81	5.07	1.27	-3.57
0.83	2.13	-0.55	1.90	1.75	-1.29	2.98	1.34	-2.07	4.03	1.24	-2.83	5.08	1.32	-3.58
0.85	2.06	-0.56	1.92	1.65	-1.31	3.00	1.32	-2.08	4.05	1.28	-2.84	5.10	1.37	-3.59

Table 3 continued

t (s)	x (cm)	y (cm)	t (s)	x (cm)	y (cm)	t (s)	x (cm)	y (cm)	t (s)	x (cm)	y (cm)
5.11	1.43	-3.60	6.12	1.38	-4.31	7.13	1.30	-5.02	8.09	0.98	-5.71
5.12	1.50	-3.61	6.14	1.45	-4.32	7.14	1.37	-5.03	8.10	1.04	-5.72
5.14	1.56	-3.62	6.15	1.51	-4.33	7.16	1.43	-5.04	8.11	1.10	-5.72
5.15	1.62	-3.63	6.17	1.57	-4.34	7.18	1.48	-5.05	8.12	1.15	-5.73
5.16	1.67	-3.63	6.18	1.61	-4.35	7.20	1.52	-5.06	8.14	1.21	-5.74
5.18	1.73	-3.64	6.21	1.67	-4.36	7.22	1.55	-5.06	8.16	1.28	-5.75
5.21	1.78	-3.65	6.23	1.70	-4.37	7.24	1.56	-5.07	8.18	1.33	-5.75
5.23	1.81	-3.66	6.26	1.69	-4.38	7.26	1.55	-5.08	8.20	1.38	-5.76
5.25	1.82	-3.67	6.29	1.66	-4.39	7.28	1.52	-5.09	8.22	1.40	-5.77
5.27	1.80	-3.68	6.31	1.60	-4.40	7.30	1.48	-5.09	8.24	1.41	-5.77
5.30	1.76	-3.69	6.33	1.53	-4.41	7.32	1.41	-5.10	8.26	1.39	-5.78
5.32	1.69	-3.70	6.35	1.45	-4.42	7.34	1.33	-5.11	8.28	1.36	-5.79
5.34	1.60	-3.71	6.37	1.35	-4.43	7.36	1.23	-5.12	8.30	1.30	-5.80
5.36	1.51	-3.72	6.39	1.25	-4.44	7.39	1.13	-5.14	8.33	1.23	-5.80
5.39	1.42	-3.74	6.41	1.14	-4.46	7.41	1.02	-5.15	8.35	1.14	-5.81
5.41	1.32	-3.75	6.43	1.05	-4.48	7.43	0.92	-5.17	8.37	1.04	-5.82
5.43	1.23	-3.77	6.46	0.97	-4.50	7.45	0.83	-5.20	8.39	0.93	-5.84
5.44	1.15	-3.78	6.47	0.94	-4.51	7.46	0.80	-5.21	8.41	0.85	-5.85
5.46	1.09	-3.80	6.48	0.91	-4.53	7.47	0.78	-5.23	8.43	0.77	-5.87
5.48	1.05	-3.82	6.49	0.90	-4.55	7.49	0.76	-5.24	8.44	0.70	-5.88
5.49	1.03	-3.84	6.51	0.91	-4.56	7.50	0.76	-5.26	8.46	0.64	-5.90
5.51	1.04	-3.86	6.52	0.92	-4.58	7.51	0.77	-5.27	8.47	0.62	-5.92
5.52	1.05	-3.87	6.53	0.95	-4.59	7.52	0.79	-5.29	8.48	0.60	-5.94
5.53	1.07	-3.89	6.54	0.99	-4.61	7.53	0.83	-5.30	8.49	0.60	-5.95
5.54	1.11	-3.90	6.56	1.04	-4.62	7.54	0.87	-5.32	8.50	0.60	-5.97
5.56	1.16	-3.91	6.57	1.08	-4.63	7.55	0.91	-5.33	8.51	0.62	-5.98
5.57	1.21	-3.92	6.58	1.13	-4.64	7.56	0.95	-5.34	8.52	0.64	-6.00
5.58	1.26	-3.94	6.59	1.18	-4.65	7.58	1.00	-5.35	8.53	0.67	-6.01
5.60	1.32	-3.95	6.60	1.24	-4.66	7.59	1.05	-5.35	8.54	0.71	-6.02
5.61	1.38	-3.95	6.61	1.30	-4.66	7.60	1.11	-5.36	8.55	0.75	-6.03
5.62	1.44	-3.96	6.63	1.36	-4.67	7.61	1.17	-5.37	8.56	0.79	-6.04
5.63	1.50	-3.97	6.64	1.42	-4.68	7.62	1.22	-5.38	8.57	0.83	-6.05
5.65	1.55	-3.98	6.66	1.47	-4.69	7.64	1.27	-5.38	8.58	0.88	-6.06
5.67	1.62	-3.99	6.68	1.54	-4.70	7.66	1.34	-5.39	8.59	0.94	-6.07
5.68	1.68	-4.00	6.70	1.59	-4.70	7.67	1.40	-5.40	8.60	0.99	-6.07
5.70	1.72	-4.00	6.72	1.62	-4.71	7.69	1.45	-5.41	8.62	1.05	-6.08
5.72	1.75	-4.01	6.74	1.63	-4.72	7.71	1.48	-5.41	8.63	1.10	-6.09
5.74	1.76	-4.02	6.77	1.62	-4.73	7.73	1.49	-5.42	8.65	1.17	-6.09
5.76	1.75	-4.03	6.79	1.58	-4.74	7.76	1.48	-5.43	8.67	1.23	-6.10
5.78	1.73	-4.04	6.82	1.51	-4.75	7.78	1.45	-5.44	8.69	1.28	-6.11
5.80	1.68	-4.04	6.84	1.41	-4.76	7.80	1.40	-5.44	8.71	1.31	-6.12
5.82	1.62	-4.05	6.86	1.32	-4.77	7.82	1.34	-5.45	8.73	1.32	-6.12
5.84	1.54	-4.06	6.88	1.22	-4.79	7.84	1.26	-5.46	8.75	1.31	-6.13
5.86	1.45	-4.07	6.90	1.12	-4.80	7.86	1.16	-5.47	8.78	1.29	-6.14
5.88	1.36	-4.09	6.92	1.02	-4.82	7.88	1.06	-5.48	8.80	1.24	-6.14
5.91	1.25	-4.10	6.94	0.96	-4.83	7.90	0.97	-5.50	8.81	1.18	-6.15
5.93	1.15	-4.12	6.95	0.91	-4.85	7.92	0.88	-5.51	8.83	1.12	-6.15
5.95	1.07	-4.14	6.97	0.87	-4.86	7.94	0.80	-5.53	8.85	1.05	-6.16
5.97	1.00	-4.16	6.98	0.84	-4.88	7.96	0.74	-5.55	8.87	0.97	-6.17
5.98	0.98	-4.18	6.99	0.83	-4.90	7.97	0.71	-5.57			
5.99	0.97	-4.19	7.01	0.84	-4.92	7.98	0.69	-5.58			
6.01	0.97	-4.21	7.02	0.86	-4.93	7.99	0.68	-5.60			
6.02	0.99	-4.23	7.03	0.90	-4.95	8.00	0.69	-5.62			
6.03	1.02	-4.24	7.05	0.94	-4.96	8.01	0.70	-5.63			
6.05	1.06	-4.26	7.06	0.98	-4.97	8.02	0.73	-5.65			
6.06	1.11	-4.27	7.07	1.03	-4.98	8.03	0.76	-5.66			
6.07	1.16	-4.28	7.08	1.08	-4.99	8.05	0.80	-5.67			
6.08	1.22	-4.29	7.09	1.13	-5.00	8.06	0.84	-5.68			
6.10	1.27	-4.30	7.10	1.19	-5.01	8.07	0.89	-5.69			
6.11	1.33	-4.31	7.11	1.24	-5.02	8.08	0.93	-5.70			

The following is the path meant to model set 2 shown in Figure 12.

Table 4: Paraboloidal Model of set 2 using MATLAB

t (s)	x (cm)	y (cm)	t (s)	x (cm)	y (cm)	t (s)	x (cm)	y (cm)	t (s)	x (cm)	y (cm)	t (s)	x (cm)	y (cm)
0.00	1.07	-0.00	0.81	1.46	-0.49	1.72	1.82	-1.15	2.62	1.69	-1.83	3.52	1.06	-2.49
0.00	1.07	-0.00	0.83	1.34	-0.50	1.74	1.75	-1.16	2.64	1.76	-1.84	3.53	1.15	-2.50
0.00	1.07	-0.00	0.85	1.22	-0.51	1.77	1.66	-1.17	2.66	1.80	-1.84	3.54	1.24	-2.51
0.00	1.07	-0.00	0.86	1.09	-0.52	1.79	1.53	-1.18	2.69	1.80	-1.85	3.55	1.32	-2.51
0.00	1.07	-0.00	0.88	0.98	-0.54	1.81	1.39	-1.19	2.71	1.77	-1.85	3.57	1.40	-2.52
0.00	1.08	-0.00	0.89	0.91	-0.55	1.83	1.27	-1.20	2.73	1.71	-1.86	3.59	1.52	-2.52
0.00	1.08	-0.00	0.91	0.85	-0.57	1.84	1.15	-1.21	2.76	1.62	-1.87	3.61	1.62	-2.53
0.00	1.09	-0.01	0.92	0.80	-0.59	1.86	1.03	-1.22	2.78	1.50	-1.87	3.64	1.69	-2.54
0.00	1.09	-0.01	0.93	0.78	-0.61	1.88	0.92	-1.24	2.80	1.35	-1.88	3.66	1.73	-2.54
0.01	1.11	-0.01	0.94	0.78	-0.63	1.89	0.85	-1.25	2.82	1.24	-1.89	3.68	1.74	-2.55
0.01	1.13	-0.01	0.95	0.80	-0.65	1.90	0.79	-1.27	2.84	1.13	-1.90	3.71	1.71	-2.55
0.01	1.16	-0.01	0.97	0.84	-0.67	1.91	0.74	-1.29	2.85	1.01	-1.91	3.73	1.65	-2.56
0.02	1.18	-0.02	0.98	0.90	-0.68	1.93	0.72	-1.31	2.87	0.89	-1.93	3.75	1.56	-2.57
0.03	1.25	-0.03	0.99	0.96	-0.70	1.94	0.71	-1.33	2.88	0.82	-1.94	3.78	1.44	-2.57
0.04	1.33	-0.03	1.00	1.02	-0.71	1.94	0.72	-1.34	2.89	0.75	-1.96	3.80	1.30	-2.58
0.05	1.40	-0.04	1.01	1.09	-0.72	1.95	0.75	-1.36	2.91	0.69	-1.98	3.82	1.14	-2.59
0.06	1.47	-0.05	1.02	1.15	-0.72	1.96	0.79	-1.37	2.92	0.66	-2.00	3.85	0.97	-2.61
0.07	1.58	-0.05	1.03	1.23	-0.73	1.97	0.83	-1.39	2.93	0.65	-2.02	3.86	0.91	-2.62
0.09	1.67	-0.06	1.04	1.31	-0.74	1.98	0.89	-1.40	2.94	0.65	-2.03	3.86	0.85	-2.62
0.11	1.75	-0.07	1.05	1.39	-0.75	1.99	0.95	-1.41	2.94	0.67	-2.05	3.87	0.80	-2.63
0.12	1.83	-0.07	1.06	1.46	-0.75	2.00	1.01	-1.42	2.95	0.69	-2.07	3.88	0.74	-2.64
0.15	1.92	-0.08	1.08	1.58	-0.76	2.01	1.08	-1.43	2.96	0.73	-2.08	3.89	0.70	-2.65
0.18	1.96	-0.09	1.10	1.67	-0.77	2.02	1.15	-1.43	2.97	0.78	-2.09	3.90	0.65	-2.66
0.21	1.95	-0.10	1.12	1.76	-0.77	2.03	1.22	-1.44	2.98	0.84	-2.11	3.90	0.62	-2.68
0.24	1.88	-0.11	1.13	1.82	-0.78	2.04	1.29	-1.45	2.99	0.90	-2.12	3.91	0.59	-2.69
0.26	1.80	-0.11	1.16	1.88	-0.79	2.06	1.40	-1.45	3.00	0.96	-2.12	3.92	0.58	-2.71
0.28	1.68	-0.12	1.18	1.90	-0.79	2.07	1.50	-1.46	3.01	1.02	-2.13	3.93	0.58	-2.73
0.31	1.54	-0.13	1.20	1.89	-0.80	2.09	1.58	-1.47	3.02	1.09	-2.14	3.94	0.59	-2.75
0.33	1.38	-0.15	1.22	1.85	-0.81	2.10	1.66	-1.47	3.03	1.15	-2.14	3.95	0.61	-2.76
0.35	1.26	-0.16	1.25	1.77	-0.81	2.13	1.77	-1.48	3.04	1.25	-2.15	3.95	0.64	-2.78
0.36	1.14	-0.17	1.27	1.67	-0.82	2.16	1.83	-1.49	3.05	1.34	-2.16	3.96	0.67	-2.79
0.38	1.02	-0.19	1.29	1.55	-0.83	2.19	1.84	-1.50	3.07	1.43	-2.16	3.97	0.72	-2.80
0.40	0.92	-0.21	1.32	1.40	-0.84	2.22	1.79	-1.50	3.08	1.51	-2.17	3.98	0.76	-2.81
0.41	0.87	-0.22	1.33	1.28	-0.85	2.24	1.72	-1.51	3.11	1.63	-2.18	3.98	0.81	-2.82
0.42	0.84	-0.24	1.35	1.16	-0.86	2.27	1.60	-1.52	3.13	1.72	-2.18	3.99	0.87	-2.83
0.43	0.81	-0.25	1.37	1.04	-0.87	2.29	1.46	-1.53	3.16	1.76	-2.19	4.00	0.92	-2.83
0.44	0.81	-0.27	1.38	0.93	-0.89	2.32	1.29	-1.54	3.19	1.77	-2.20	4.01	0.98	-2.84
0.45	0.82	-0.29	1.39	0.86	-0.90	2.33	1.18	-1.55	3.21	1.73	-2.21	4.02	1.07	-2.85
0.46	0.85	-0.31	1.41	0.81	-0.92	2.35	1.07	-1.56	3.24	1.64	-2.21	4.03	1.15	-2.85
0.47	0.89	-0.32	1.42	0.77	-0.94	2.37	0.95	-1.58	3.27	1.51	-2.22	4.04	1.23	-2.86
0.48	0.94	-0.33	1.43	0.75	-0.96	2.38	0.85	-1.59	3.30	1.35	-2.23	4.06	1.31	-2.86
0.49	0.99	-0.35	1.44	0.75	-0.98	2.39	0.79	-1.61	3.32	1.24	-2.24	4.08	1.43	-2.87
0.50	1.05	-0.35	1.45	0.77	-1.00	2.40	0.74	-1.62	3.33	1.12	-2.25	4.10	1.53	-2.88
0.51	1.11	-0.36	1.46	0.81	-1.02	2.42	0.70	-1.64	3.35	1.00	-2.26	4.12	1.61	-2.88
0.52	1.17	-0.37	1.48	0.87	-1.04	2.43	0.68	-1.66	3.36	0.89	-2.27	4.14	1.66	-2.89
0.53	1.25	-0.38	1.49	0.92	-1.05	2.44	0.68	-1.68	3.38	0.81	-2.29	4.16	1.70	-2.89
0.54	1.33	-0.39	1.49	0.98	-1.06	2.45	0.70	-1.70	3.39	0.73	-2.30	4.19	1.69	-2.90
0.55	1.41	-0.39	1.50	1.05	-1.07	2.46	0.74	-1.72	3.40	0.67	-2.32	4.21	1.66	-2.91
0.56	1.48	-0.40	1.51	1.11	-1.07	2.47	0.79	-1.74	3.41	0.63	-2.34	4.24	1.59	-2.91
0.58	1.59	-0.41	1.52	1.19	-1.08	2.48	0.85	-1.75	3.42	0.61	-2.36	4.26	1.49	-2.92
0.60	1.69	-0.41	1.54	1.27	-1.09	2.49	0.90	-1.76	3.43	0.61	-2.38	4.28	1.36	-2.93
0.61	1.78	-0.42	1.55	1.35	-1.10	2.50	0.96	-1.77	3.44	0.62	-2.39	4.31	1.20	-2.94
0.63	1.84	-0.43	1.56	1.42	-1.10	2.51	1.03	-1.78	3.45	0.64	-2.41	4.33	1.04	-2.95
0.65	1.90	-0.43	1.58	1.53	-1.11	2.52	1.10	-1.78	3.46	0.68	-2.43	4.35	0.93	-2.96
0.68	1.93	-0.44	1.59	1.63	-1.12	2.53	1.18	-1.79	3.46	0.72	-2.44	4.36	0.82	-2.97
0.70	1.92	-0.45	1.61	1.71	-1.12	2.54	1.25	-1.80	3.47	0.77	-2.45	4.38	0.72	-2.99
0.72	1.89	-0.45	1.63	1.78	-1.13	2.55	1.32	-1.80	3.48	0.82	-2.46	4.39	0.63	-3.01
0.74	1.82	-0.46	1.65	1.84	-1.14	2.57	1.43	-1.81	3.49	0.88	-2.47	4.40	0.59	-3.02
0.77	1.73	-0.47	1.67	1.87	-1.14	2.58	1.54	-1.82	3.50	0.94	-2.48	4.41	0.56	-3.04
0.79	1.60	-0.48	1.70	1.86	-1.15	2.60	1.62	-1.82	3.51	1.00	-2.48	4.42	0.55	-3.05

Table 4 continued

t (s)	x (cm)	y (cm)	t (s)	x (cm)	y (cm)	t (s)	x (cm)	y (cm)
4.42	0.54	-3.07	5.34	0.87	-3.65	6.06	1.23	-4.28
4.43	0.54	-3.09	5.35	0.78	-3.66	6.09	1.38	-4.28
4.44	0.56	-3.11	5.37	0.69	-3.68	6.12	1.48	-4.29
4.45	0.58	-3.12	5.38	0.61	-3.69	6.15	1.54	-4.30
4.46	0.62	-3.14	5.39	0.54	-3.71	6.18	1.54	-4.30
4.46	0.66	-3.15	5.40	0.50	-3.73	6.21	1.50	-4.31
4.47	0.70	-3.16	5.41	0.48	-3.74	6.23	1.43	-4.31
4.48	0.75	-3.17	5.41	0.46	-3.76	6.25	1.33	-4.32
4.48	0.80	-3.17	5.42	0.46	-3.78	6.28	1.20	-4.32
4.49	0.86	-3.18	5.43	0.47	-3.79	6.30	1.10	-4.33
4.50	0.92	-3.19	5.44	0.48	-3.81	6.31	0.98	-4.33
4.51	0.98	-3.19	5.44	0.51	-3.83	6.33	0.86	-4.34
4.52	1.05	-3.20	5.45	0.54	-3.84	6.35	0.73	-4.35
4.53	1.15	-3.21	5.46	0.58	-3.85	6.36	0.65	-4.36
4.55	1.24	-3.21	5.46	0.61	-3.86	6.37	0.57	-4.38
4.56	1.33	-3.22	5.47	0.66	-3.87	6.38	0.50	-4.39
4.58	1.41	-3.22	5.48	0.70	-3.88	6.39	0.44	-4.41
4.61	1.54	-3.23	5.49	0.76	-3.88	6.40	0.41	-4.43
4.64	1.62	-3.24	5.49	0.82	-3.89	6.40	0.39	-4.44
4.66	1.66	-3.25	5.50	0.88	-3.90	6.41	0.38	-4.46
4.69	1.65	-3.25	5.51	0.94	-3.90	6.42	0.37	-4.48
4.72	1.59	-3.26	5.52	1.03	-3.91	6.42	0.38	-4.49
4.75	1.48	-3.27	5.54	1.13	-3.92	6.43	0.39	-4.51
4.78	1.33	-3.27	5.55	1.21	-3.92	6.44	0.41	-4.53
4.81	1.15	-3.29	5.57	1.29	-3.93	6.44	0.44	-4.54
4.82	1.06	-3.29	5.60	1.43	-3.93	6.45	0.47	-4.55
4.84	0.96	-3.30	5.63	1.53	-3.94	6.45	0.50	-4.56
4.85	0.85	-3.31	5.65	1.58	-3.95	6.46	0.54	-4.57
4.86	0.75	-3.32	5.68	1.58	-3.95	6.47	0.58	-4.58
4.87	0.68	-3.34	5.71	1.54	-3.96	6.47	0.63	-4.58
4.89	0.62	-3.35	5.73	1.47	-3.96	6.48	0.68	-4.59
4.90	0.56	-3.37	5.76	1.37	-3.97	6.49	0.73	-4.60
4.91	0.52	-3.39	5.78	1.24	-3.97	6.49	0.78	-4.60
4.91	0.51	-3.40	5.80	1.13	-3.98	6.51	0.87	-4.61
4.92	0.50	-3.42	5.82	1.01	-3.99	6.52	0.95	-4.61
4.93	0.50	-3.44	5.83	0.89	-4.00	6.53	1.04	-4.62
4.94	0.52	-3.46	5.85	0.76	-4.01	6.54	1.11	-4.62
4.94	0.54	-3.47	5.86	0.68	-4.02	6.57	1.26	-4.63
4.95	0.58	-3.49	5.87	0.60	-4.03	6.60	1.37	-4.64
4.96	0.62	-3.50	5.88	0.53	-4.05	6.62	1.45	-4.64
4.97	0.66	-3.51	5.90	0.47	-4.07	6.65	1.49	-4.65
4.98	0.71	-3.52	5.90	0.45	-4.08	6.65	1.50	-4.65
4.98	0.76	-3.53	5.91	0.43	-4.10	6.66	1.50	-4.65
4.99	0.81	-3.53	5.92	0.42	-4.12	6.66	1.50	-4.65
5.00	0.86	-3.54	5.92	0.42	-4.13	6.67	1.50	-4.65
5.01	0.94	-3.55	5.93	0.43	-4.15			
5.02	1.02	-3.55	5.94	0.44	-4.17			
5.03	1.10	-3.56	5.94	0.47	-4.18			
5.04	1.17	-3.56	5.95	0.50	-4.19			
5.06	1.29	-3.57	5.95	0.53	-4.20			
5.08	1.40	-3.58	5.96	0.57	-4.21			
5.10	1.48	-3.58	5.97	0.61	-4.22			
5.12	1.55	-3.59	5.97	0.65	-4.23			
5.15	1.61	-3.59	5.98	0.71	-4.24			
5.18	1.62	-3.60	5.99	0.76	-4.24			
5.21	1.57	-3.61	6.00	0.82	-4.25			
5.24	1.47	-3.61	6.01	0.88	-4.25			
5.27	1.35	-3.62	6.02	0.97	-4.26			
5.29	1.21	-3.63	6.03	1.07	-4.27			
5.32	1.05	-3.64	6.05	1.15	-4.27			

9 Appendix C: Neural Network Data

The following is the data generated by the neural network (Figure 20) meant to model set 1.

Table 5: Neural Network Model of set 1

t (s)	x (cm)	y (cm)	t (s)	x (cm)	y (cm)	t (s)	x (cm)	y (cm)	t (s)	x (cm)	y (cm)	t (s)	x (cm)	y (cm)
0.00	-12.59	-2.80	2.00	12.14	4.82	4.00	-0.93	0.77	6.00	-0.04	0.29	8.00	-0.03	0.29
0.03	2.81	-11.01	2.03	14.92	3.34	4.03	-0.86	0.73	6.03	-0.04	0.29	8.03	-0.03	0.29
0.07	40.09	2.41	2.07	17.64	1.81	4.07	-0.79	0.69	6.07	-0.04	0.29	8.07	-0.03	0.29
0.10	42.34	0.38	2.10	19.80	0.13	4.10	-0.73	0.66	6.10	-0.04	0.29	8.10	-0.03	0.29
0.13	-20.98	17.39	2.13	18.63	-2.43	4.13	-0.67	0.63	6.13	-0.03	0.29	8.13	-0.03	0.29
0.17	-3.70	13.19	2.17	7.23	-7.67	4.17	-0.61	0.60	6.17	-0.03	0.29	8.17	-0.03	0.29
0.20	7.46	10.46	2.20	-5.02	-13.13	4.20	-0.57	0.57	6.20	-0.03	0.29	8.20	-0.03	0.29
0.23	10.74	9.65	2.23	-6.79	-15.81	4.23	-0.52	0.55	6.23	-0.03	0.29	8.23	-0.03	0.29
0.27	11.51	9.44	2.27	-4.84	-17.43	4.27	-0.48	0.53	6.27	-0.03	0.29	8.27	-0.03	0.29
0.30	11.73	9.35	2.30	-2.84	-18.05	4.30	-0.44	0.51	6.30	-0.03	0.29	8.30	-0.03	0.29
0.33	11.86	9.28	2.33	-7.39	-9.33	4.33	-0.41	0.49	6.33	-0.03	0.29	8.33	-0.03	0.29
0.37	11.99	9.18	2.37	-19.09	9.45	4.37	-0.38	0.47	6.37	-0.03	0.29	8.37	-0.03	0.29
0.40	12.17	8.99	2.40	-19.16	11.77	4.40	-0.35	0.46	6.40	-0.03	0.29	8.40	-0.03	0.29
0.43	12.48	8.56	2.43	-16.87	10.71	4.43	-0.32	0.44	6.43	-0.03	0.29	8.43	-0.03	0.29
0.47	13.09	7.39	2.47	-14.50	9.47	4.47	-0.30	0.43	6.47	-0.03	0.29	8.47	-0.03	0.29
0.50	10.84	-6.60	2.50	-12.20	8.25	4.50	-0.27	0.42	6.50	-0.03	0.29	8.50	-0.03	0.29
0.53	-5.88	-73.23	2.53	-10.00	7.09	4.53	-0.25	0.41	6.53	-0.03	0.29	8.53	-0.01	0.30
0.57	-0.49	-88.20	2.57	-7.89	5.98	4.57	-0.23	0.40	6.57	-0.03	0.29	8.57	0.11	0.32
0.60	6.89	-103.71	2.60	-5.88	4.91	4.60	-0.22	0.39	6.60	-0.03	0.29	8.60	0.75	0.46
0.63	8.27	-112.68	2.63	-3.97	3.90	4.63	-0.20	0.38	6.63	-0.03	0.29	8.63	3.14	0.98
0.67	-6.20	-10.19	2.67	-2.15	2.94	4.67	-0.19	0.37	6.67	-0.03	0.29	8.67	6.36	1.69
0.70	-21.50	-3.90	2.70	-0.42	2.03	4.70	-0.17	0.37	6.70	-0.03	0.29	8.70	7.64	1.97
0.73	-22.79	-6.15	2.73	1.21	1.17	4.73	-0.16	0.36	6.73	-0.03	0.29	8.73	7.91	2.02
0.77	-22.11	-6.21	2.77	2.74	0.35	4.77	-0.15	0.35	6.77	-0.03	0.29	8.77	7.95	2.03
0.80	-19.80	-3.94	2.80	4.19	-0.41	4.80	-0.14	0.35	6.80	-0.03	0.29	8.80	7.96	2.04
0.83	-13.57	3.58	2.83	5.54	-1.13	4.83	-0.13	0.34	6.83	-0.03	0.29	8.83	7.96	2.04
0.87	-7.29	11.13	2.87	6.81	-1.80	4.87	-0.12	0.34	6.87	-0.03	0.29			
0.90	-4.91	13.48	2.90	8.00	-2.43	4.90	-0.12	0.34	6.90	-0.03	0.29			
0.93	-4.03	13.72	2.93	9.11	-3.01	4.93	-0.11	0.33	6.93	-0.03	0.29			
0.97	-3.38	13.49	2.97	10.14	-3.56	4.97	-0.10	0.33	6.97	-0.03	0.29			
1.00	-2.65	13.10	3.00	11.08	-4.06	5.00	-0.10	0.33	7.00	-0.03	0.29			
1.03	-1.68	12.55	3.03	11.88	-4.48	5.03	-0.09	0.32	7.03	-0.03	0.29			
1.07	-0.29	11.72	3.07	12.31	-4.74	5.07	-0.09	0.32	7.07	-0.03	0.29			
1.10	1.86	10.41	3.10	11.70	-4.51	5.10	-0.08	0.32	7.10	-0.03	0.29			
1.13	5.33	8.25	3.13	8.41	-3.04	5.13	-0.08	0.32	7.13	-0.03	0.29			
1.17	10.94	4.72	3.17	1.96	-0.11	5.17	-0.07	0.31	7.17	-0.03	0.29			
1.20	19.49	-0.71	3.20	-3.42	2.33	5.20	-0.07	0.31	7.20	-0.03	0.29			
1.23	31.05	-8.07	3.23	-5.46	3.24	5.23	-0.07	0.31	7.23	-0.03	0.29			
1.27	43.92	-16.36	3.27	-5.75	3.33	5.27	-0.06	0.31	7.27	-0.03	0.29			
1.30	49.97	-22.12	3.30	-5.48	3.18	5.30	-0.06	0.31	7.30	-0.03	0.29			
1.33	6.92	-11.00	3.33	-5.09	2.97	5.33	-0.06	0.31	7.33	-0.03	0.29			
1.37	-17.49	-5.01	3.37	-4.70	2.76	5.37	-0.06	0.30	7.37	-0.03	0.29			
1.40	-15.14	-7.04	3.40	-4.32	2.56	5.40	-0.05	0.30	7.40	-0.03	0.29			
1.43	-12.17	-8.83	3.43	-3.97	2.37	5.43	-0.05	0.30	7.43	-0.03	0.29			
1.47	-9.85	-10.16	3.47	-3.65	2.20	5.47	-0.05	0.30	7.47	-0.03	0.29			
1.50	-7.88	-11.25	3.50	-3.35	2.05	5.50	-0.05	0.30	7.50	-0.03	0.29			
1.53	-6.07	-12.19	3.53	-3.08	1.90	5.53	-0.05	0.30	7.53	-0.03	0.29			
1.57	-4.38	-12.85	3.57	-2.83	1.77	5.57	-0.05	0.30	7.57	-0.03	0.29			
1.60	-3.16	-12.30	3.60	-2.60	1.65	5.60	-0.04	0.30	7.60	-0.03	0.29			
1.63	-3.79	-7.08	3.63	-2.38	1.53	5.63	-0.04	0.30	7.63	-0.03	0.29			
1.67	-7.13	4.95	3.67	-2.19	1.43	5.67	-0.04	0.30	7.67	-0.03	0.29			
1.70	-8.85	13.17	3.70	-2.01	1.34	5.70	-0.04	0.30	7.70	-0.03	0.29			
1.73	-7.82	14.80	3.73	-1.84	1.25	5.73	-0.04	0.30	7.73	-0.03	0.29			
1.77	-5.79	14.19	3.77	-1.69	1.17	5.77	-0.04	0.30	7.77	-0.03	0.29			
1.80	-3.49	13.06	3.80	-1.56	1.10	5.80	-0.04	0.30	7.80	-0.03	0.29			
1.83	-1.07	11.80	3.83	-1.43	1.03	5.83	-0.04	0.29	7.83	-0.03	0.29			
1.87	1.44	10.47	3.87	-1.31	0.97	5.87	-0.04	0.29	7.87	-0.03	0.29			
1.90	4.02	9.11	3.90	-1.20	0.91	5.90	-0.04	0.29	7.90	-0.03	0.29			
1.93	6.67	7.71	3.93	-1.11	0.86	5.93	-0.04	0.29	7.93	-0.03	0.29			
1.97	9.38	6.28	3.97	-1.02	0.81	5.97	-0.04	0.29	7.97	-0.03	0.29			